3. THE FLOW BENEATH A FORMULA ONE RACING CAR

The floor of a Formula One racing car is potentially an area where notable aerodynamic gains can be made. The floor can roughly contribute a third of the total downforce[27]. In addition, the pressure distribution under the floor also influences the centre of pressure and related pitch sensitivity of the car. An understanding of these flow patterns and resulting forces can therefore be very useful in optimising aerodynamic performance. The flow beneath an F1 car was therefore investigated.

For this research project, a 30 % scale model of the Parmalat Forti Ford FG01-95 F1 racing car was used. The full-scale car was raced in the 1995 F.I.A. governed[45] F1 world championship.

Both experimental and numerical techniques were used. The experimental part of this study was aimed at capturing the 3D flow field, while the numerical side was directed at reproducing the floor centre-line pressure distribution.

To curb the high levels of traction obtained using *ground effects*, the F.I.A. have laid down strict rules governing the shape of the car floor. Although these rules[45] have not been repeated here, the "rule box" is presented in Figure 3-1. This is the envelope into which all sprung parts of the car have to fit. It has been inverted to show the floor area.

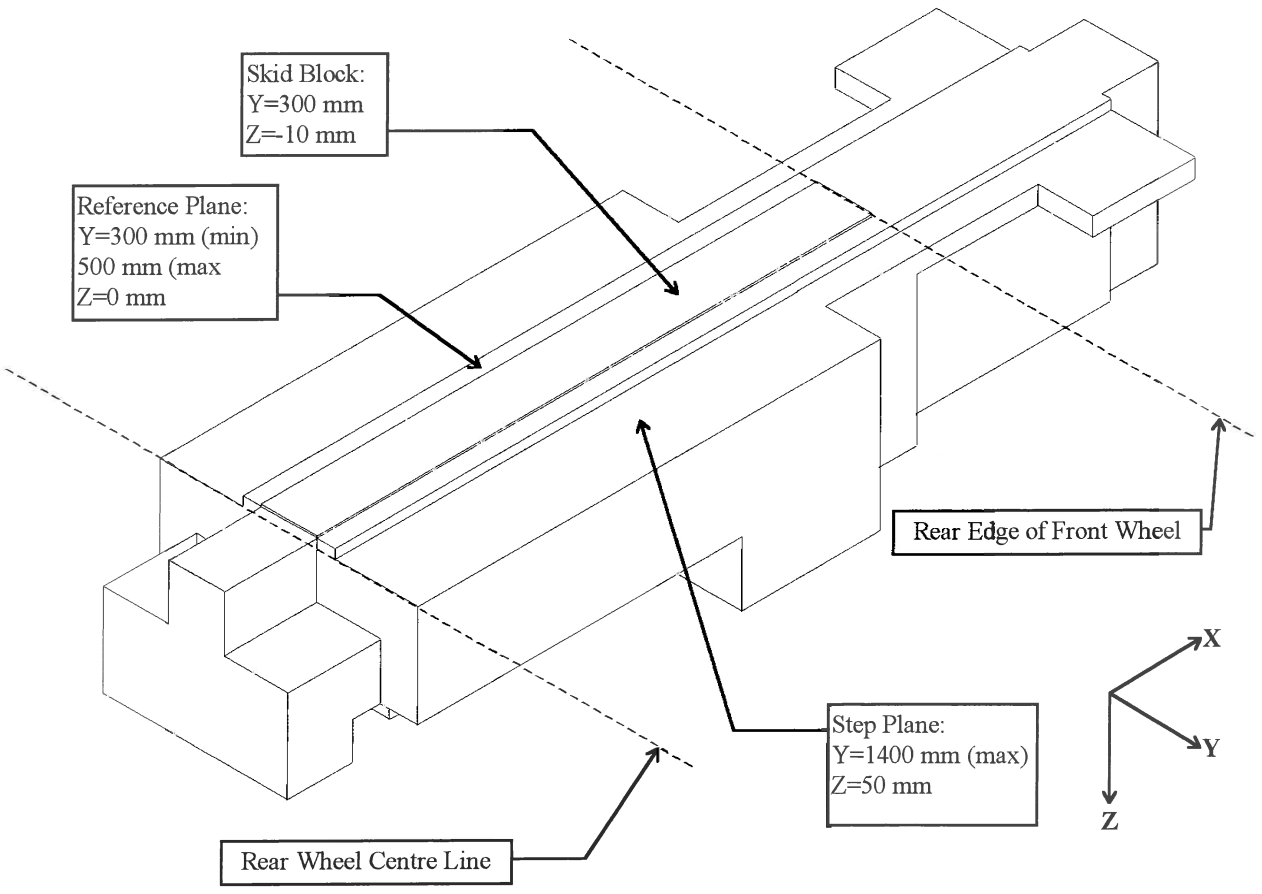

Figure 3-1 Representation of the 1995 FIA Formula One Rule Box

The resulting car floor, designed using the constraints of Figure 3-1, is shown in Figure 3-2.

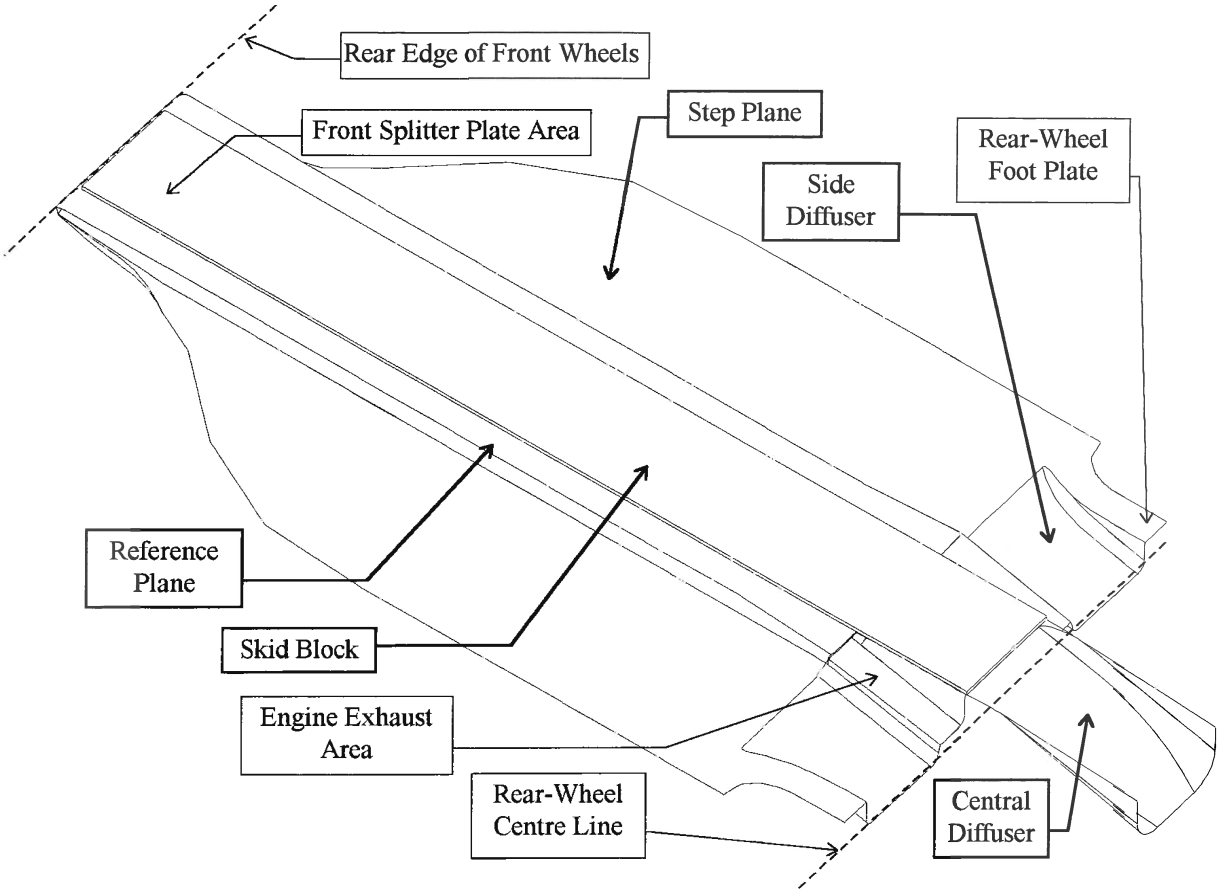

Figure 3-2 Inverted view of the floor

3.1 Experimental Investigation

The experimental investigation was aimed at characterising the centre-line flow pattern and then determining which factors, external to the floor, were predominantly responsible for the 3D pressure distribution under the floor of the car. This was achieved by using a baseline model as a reference and then varying certain parameters. As the fundamental flow pattern was the sole concern of this study, the model changes were selected to induce large shifts in the pitch and downforce of the car. Three sets of experiments were chosen to satisfy this criteria. These were:

- Model ride height and angle of attack variations
- Front-flap angle adjustments
- Front and rear wheel assessments

The experimental tests were also used to obtain data for the numerical investigation as presented in section 3.2.

3.1.1 Experimental Set-up

The closed-return LSWT at the Council for Scientific and Industrial Research (CSIR) in South Africa was used for the tests. The wind tunnel had a 1.5x2.1x3.7m closed test section and was equipped with a rolling road. The maximum obtainable belt speed was 30 m/s. The wind tunnel was also equipped with an overhead six-component virtual-centre balance.

The blockage ratio, as defined in section 2.2.3.2 was calculated to be 4.1%. All tests were performed at 24 m/s. Using the length of the model as the characteristic length, the Reynolds Number was in the range of $5x10^6$. This satisfied the criteria of Barnard[16] for Reynolds-Number independence as discussed in section 2.2.3.1. A picture of the model, mounted in the tunne, is shown in Figure 3-3.

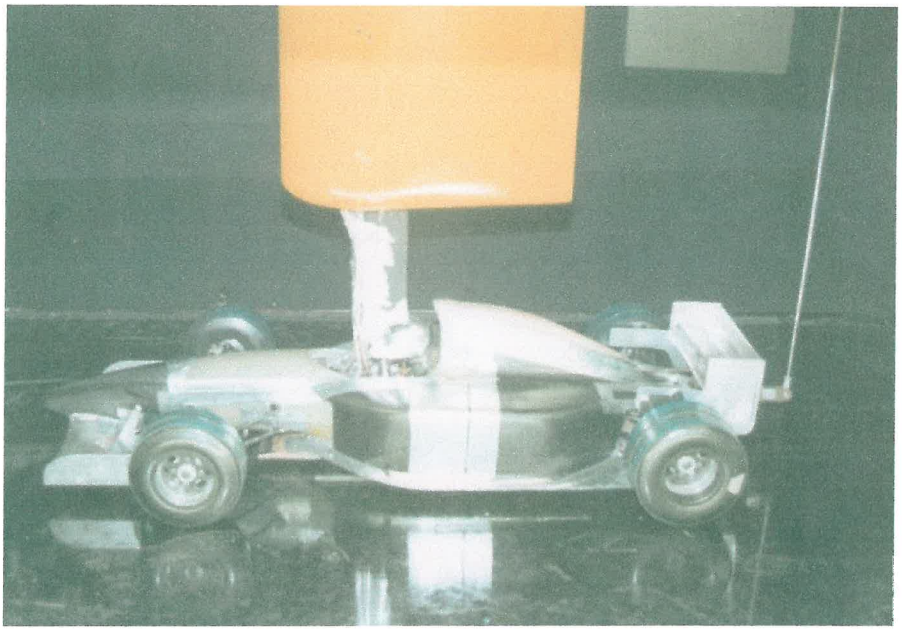

Figure 3-3 Set-up of the car in the wind tunnel

For ease of comparison with numerical data, all tunnel correction factors were removed.

The body parts of the model were made of glass and carbon fibre reinforced plastic (CFRP) using CNC machined moulds. The front and rear wings and flaps, spine, and wishbones were made of aluminium. The carbon fibre wheels were covered with a smooth, non-stick surface. The wheels were dynamically balanced before the start of the investigation. Internally, the model had a representative engine, gearbox, air intake and exhaust as well as scaled radiators. Ride height, front flap and rear wing adjustments were automated using internal stepper motors.

The CFRP floor was fitted with 92 pressure taps at locations shown in Figure 3-4. The longitudinal centre line was assumed to be the line of flow reflection.

The surface pressure tappings were constructed by drilling small holes perpendicular to the relevant surfaces and inserting metal tubes which were fixed flush to the surface to ensure no flow interference. The metal tubes were connected to two Scanivalve[vii] pressure transducers via plastic tubes. Due to the large number of plastic tubes, the Scanivalves were mounted inside the model so that only the six control cables (3 per Scanivalve) had to be taken from the model.

[vii] The Scanivalves that were used each contained a single pressure transducer with a manifold-type head which accommodated up to 48 pressure taps. All pressures were measured relative to a datum pressure. Each pressure port was measured sequentially by aligning the 48 ports with the transducer. The measured voltage signals were sent to a central processing unit where they were converted and non-dimensionalised to pressure coefficients (C_P).

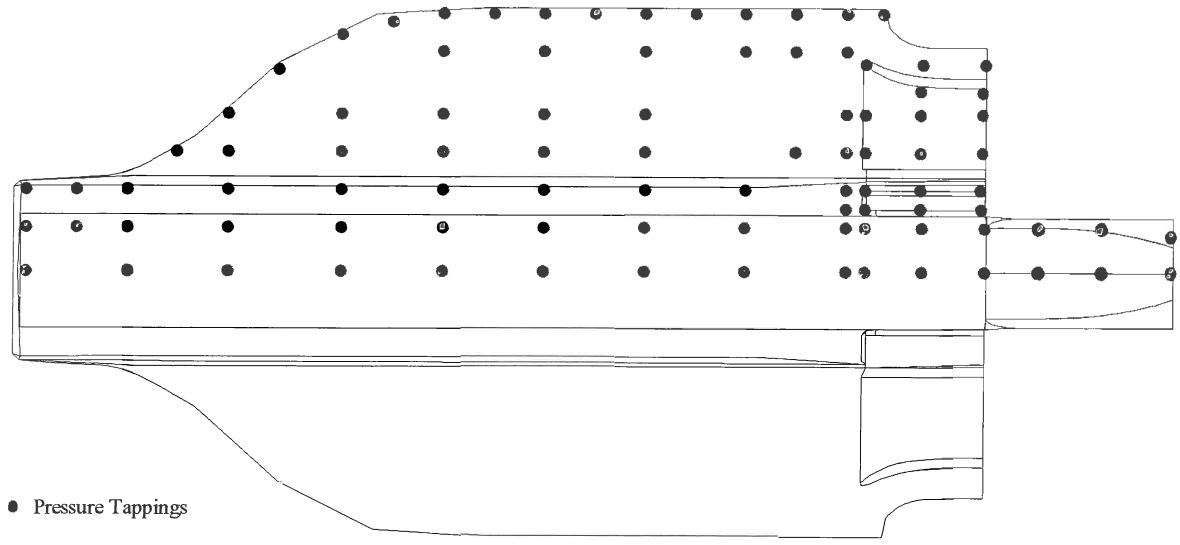

Figure 3-4 Location of pressure taps under the car floor

The wheels were mounted onto the model. Figure 3-5 shows detail of the model, the spine, the wheels, the two Scanivalves and the concealed pressure tappings.

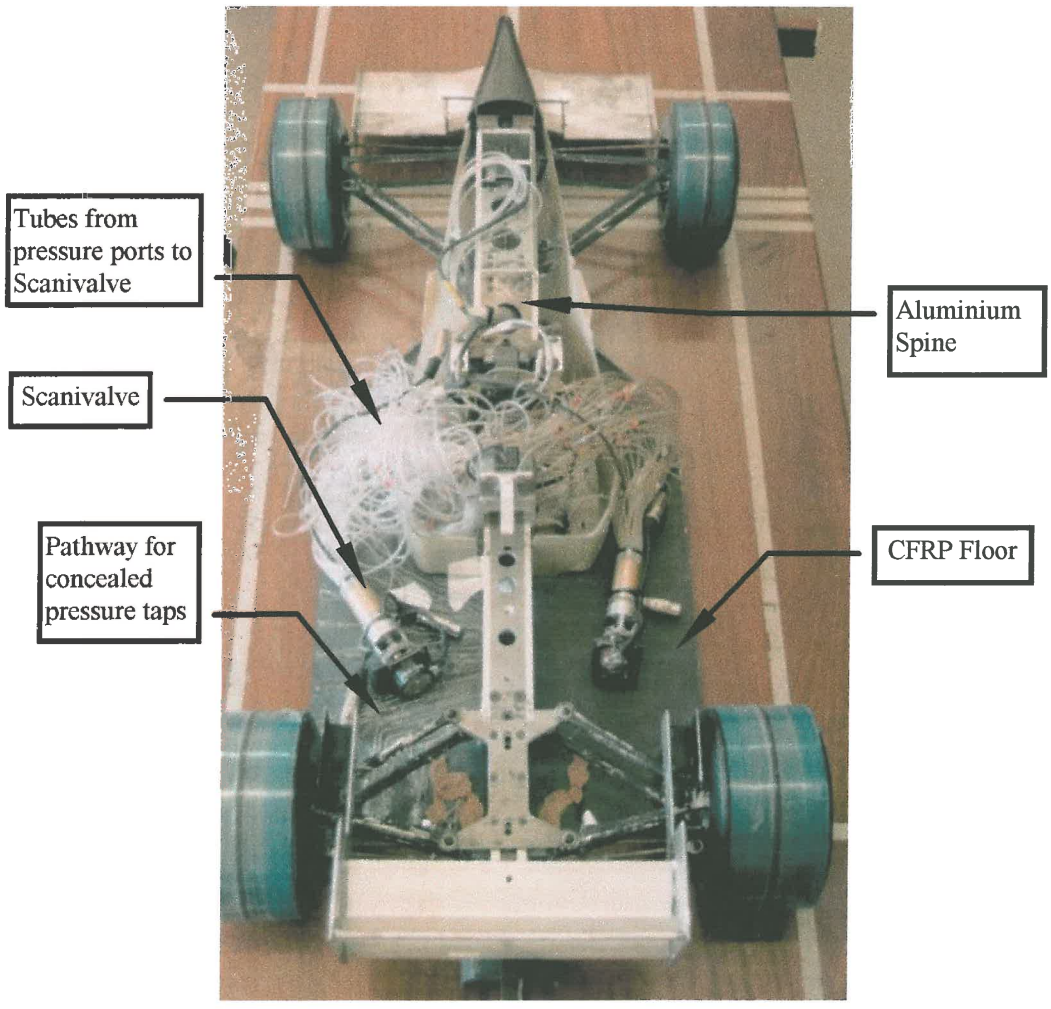

Figure 3-5 Model Construction

The adjustable components of the base-line model were fixed as summarised in Table 3-1. These remained unchanged throughout the study unless specified.

Model Parameter	Abbreviation	Value
Basic Model Configuration	-	**Standard model**
Front Ride Height (Full Scale - FS[viii])	FRH[ix]	20 mm
Rear Ride Height (Full Scale - FS)	RRH	40 mm
Front Flap Angle	FFA	9.3°
Rear Wing Angle	RWA	31°

Table 3-1 Model set-up

As an indication of the aerodynamic sensitivity to changes in the parameters listed in Table 3-1, the overhead balance was used to obtain coefficients for the complete vehicle. A 20 mm FS change in RRH would affect the COP by 5% when compared to the baseline case. Changing the FFA by 3 degrees shifted the COP by approximately 5 %. A 15 degree change in RWA changed the downforce by about 100 kg's.

3.1.2 Experimental Results

The experimental results below, are all based on pressure coefficients obtained from the scale model floor.

3.1.2.1 Repeatability

To illustrate the repeatability of the wind tunnel and model set-up, two sets of data were used. These were obtained on separate test days. The model had been modified between the two runs and was brought back to the specification as described in Table 3-1, before the second run was made. The repeatability, as summarised in Table 3-2 was only calculated for the pressure tapping. The overhead balance was not used during the tests.

Variable calculated	Result
Mean Pressure coefficient of Run 1 (C_P over 92 taps)	-1.6556
Mean Pressure coefficient of Run 2 (C_P over 92 taps)	-1.6628
Mean difference between Runs	0.0072
Mean difference expressed as a percentage (%)	0.4330

Table 3-2 Results of repeatability calculations

From the table it is evident that high levels of repeatability were achieved. Differences of less than 0.43% would have to be interpreted as repeatability errors and not as aerodynamic changes.

[viii] FS - Full Scale dimensions
MS - Model Scale dimensions

[ix] The terms front (FRH) and rear (RRH) ride height are defined as the air gap between the front and rear wheel centre lines respectively.

3.1.2.2 The Centre-Line Flow Pattern

As an introduction to the flow pattern beneath the vehicle, the centre-line pressure distribution of the baseline car is presented first.

The basic shape of a centre-line pressure distribution curve is found to be common to many smooth-bottomed, open and closed-wheel racing cars fitted with front splitters and rear diffusers[8,13]. The centre-line pressure plot of the stepped Forti floor, as presented in Figure 3-6, also exhibits these characteristics.

By inspection, the profile in Figure 3-6 can be divided into three separate curves connected by two inflection points. These can be linked directly to three physical zones on the car as shown in the figure. Zone I represents the front splitter. As found by Dominy[7], the stagnation point induced by the splitter and the proximity of the body, causes the flow to accelerate and then to diffuse downstream of the stagnation point. This is clearly indicated by the slope of the curve in Zone I.

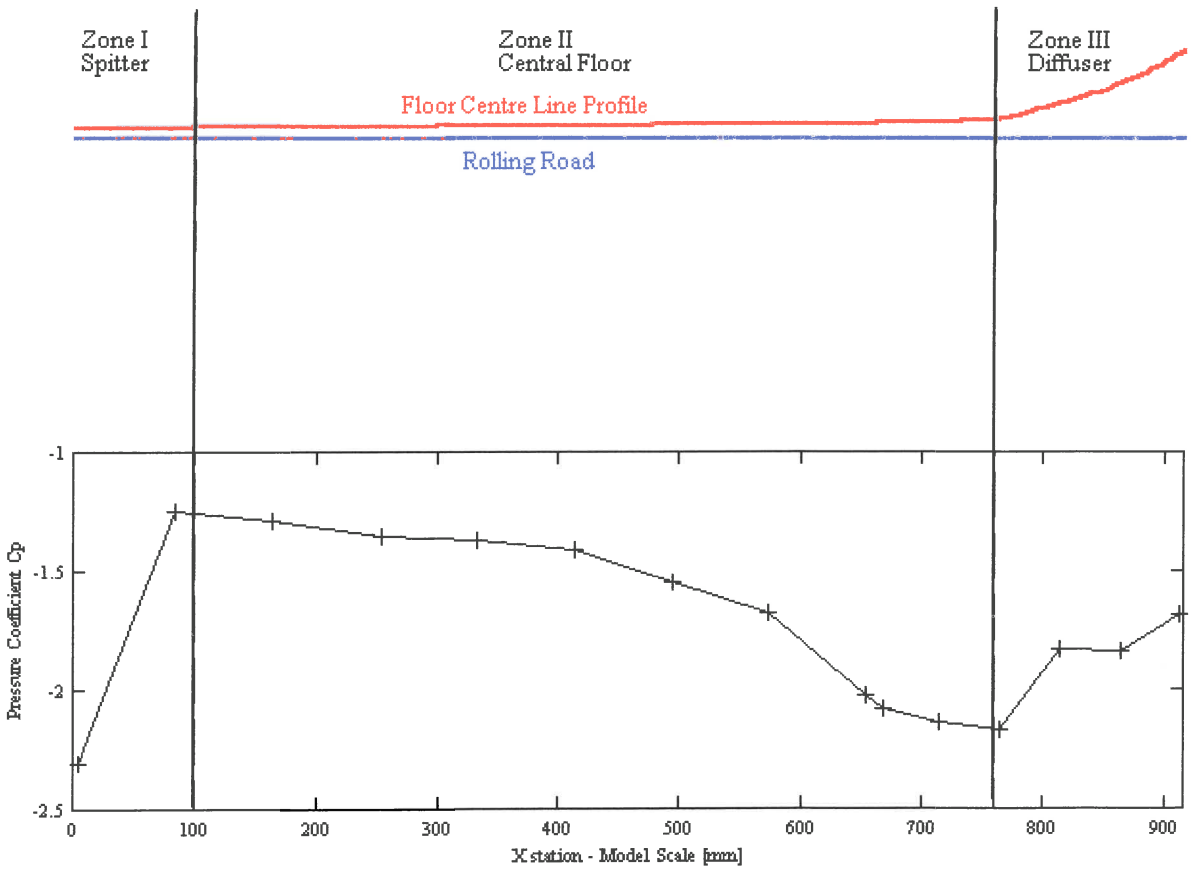

Figure 3-6 Centre-line pressure coefficient plot of the baseline set-up

Flow acceleration and diffusion are also responsible for the characteristic diffuser curve as seen in zone III. The transition from the central floor to the angled diffuser causes an area of local flow acceleration, inducing a sharp static-pressure drop. The maximum diffuser angle and corresponding negative pressures in this area are limited by the momentum of the air. Too steep an angle will cause separation, corresponding to a loss in downforce. The momentum of the air can be increased by matching the diffuser with the rear-wing assembly. When this is done correctly, the rear wing acts as a pump, energising the air and prolonging separation.

Higher diffuser angles can then be attained. As can be seen from the position of the inflection point in zone II, the effect of the rear-wing assembly and diffuser is more pronounced than the front-splitter.

Extending the conclusions regarding the shape of the pressure profile to positions away from the centre line is not obvious, as a racing car and especially a Formula One car is a highly three dimensional body. This is illustrated by the 3D pressure map in Figure 3-7[x] and the contour plot in Figure 3-8.

As anticipated, examination of the two figures reveals significant differences at stations away from the centre line. Most notable is the diffuser area which consists of a central diffuser, two side diffusers and two smaller exhaust diffusers. The transition from the reference plane to the step plane also has an influence on the contours. Other areas which are notably different, are the floor-edge area below the cooling intakes and the area immediately in front of the rear diffuser. Higher than average pressure peaks are clearly visible.

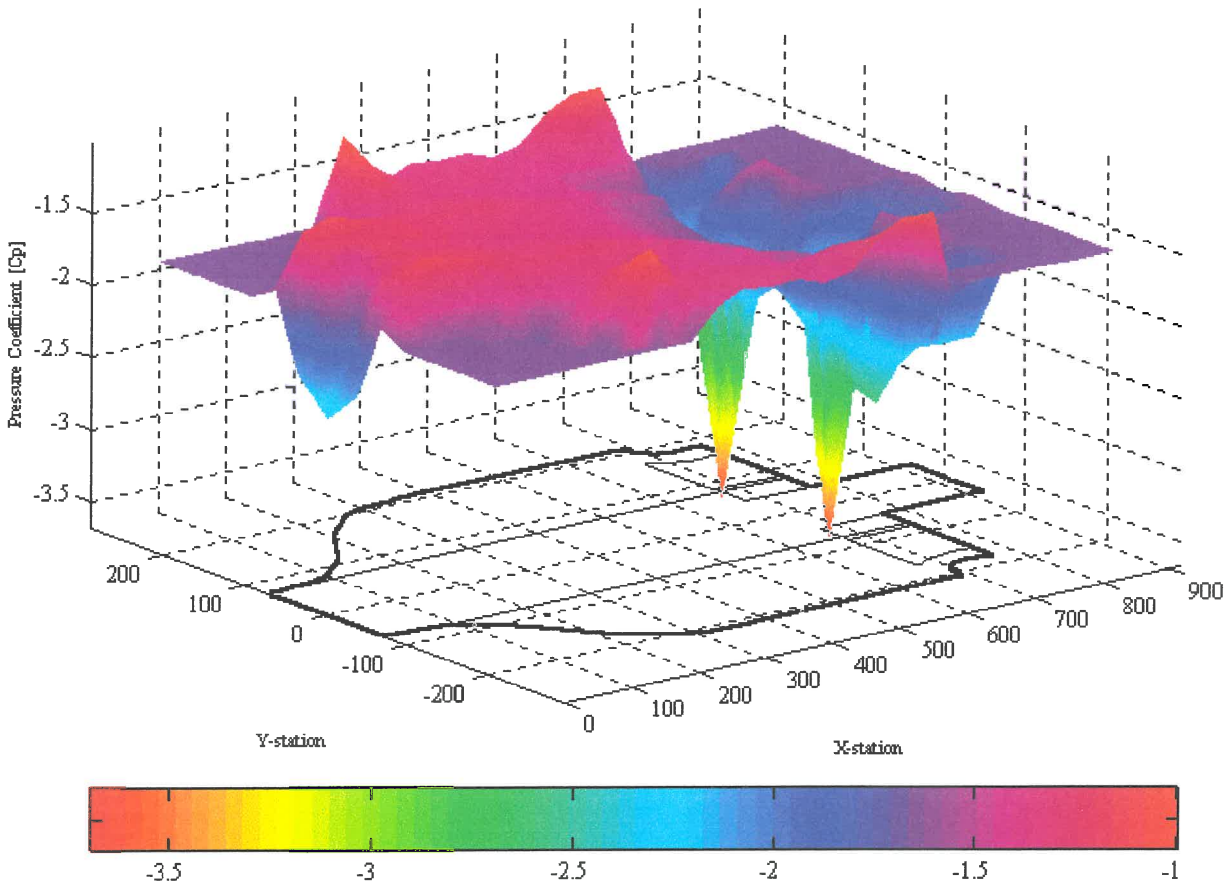

Figure 3-7 Pressure map of the floor - Baseline Model

[x] The planar area (blue/purple) of the pressure map lying outside the boundaries of the floor represent the correct position of the average pressure coefficient.

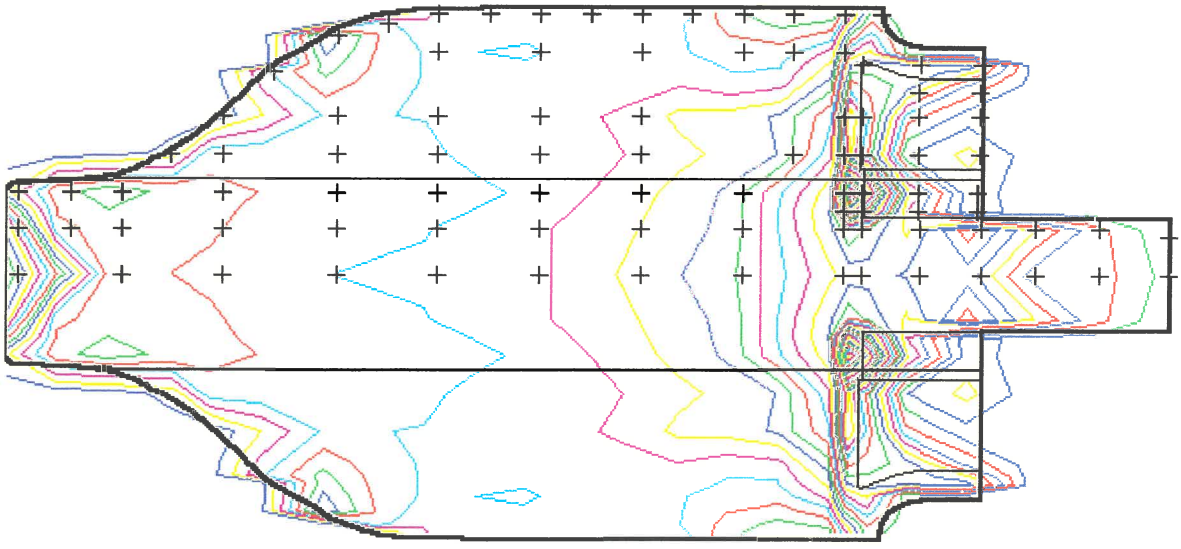

Figure 3-8 Pressure contour plot of the floor - Baseline Model

3.1.2.3 The Effect of Ride-Height Adjustments

As a first step in determining the parameters influencing the shape of the pressure map, the effect of different ride heights were investigated. Three sets of ride heights were applied to the baseline model. The ride heights, as listed in Table 3-3, were chosen to represent the dynamic operating range of the car. Diffuser stall was not induced.

Front Ride Height	Rear Ride Height	Reason
10 mm	20 mm	Minimum Ride Height
24 mm	40 mm	Static Ride Height (control)
30 mm	60 mm	Maximum Ride Height

Table 3-3 Ride Height configuration

Note that the pitch of the model and the ground clearance was varied. The C_P contour plots of the three configurations are shown in Figure 3-9[xi].

From Figure 3-9 it can be seen that the underlying flow phenomena is relatively insensitive to variations in ride height. The basic contour and position of most isobars remain relatively constant throughout the ride-height range. As expected, the ground effect reduces as the air gap is increased. It is concluded that the basic flow pattern is not fundamentally altered by variations in ride height or pitch.

It should be stressed that although the changes that are observed in the figures are significant with respect to the aerodynamic performance of the car, this investigation was aimed at finding dramatic flow-pattern changes. In this context, smaller changes are not seen as significant.

[xi] Each colour represents the same pressure value in all the plots. The practice of colour co-ordinated pressure contours will be used throughout the remainder of the text.

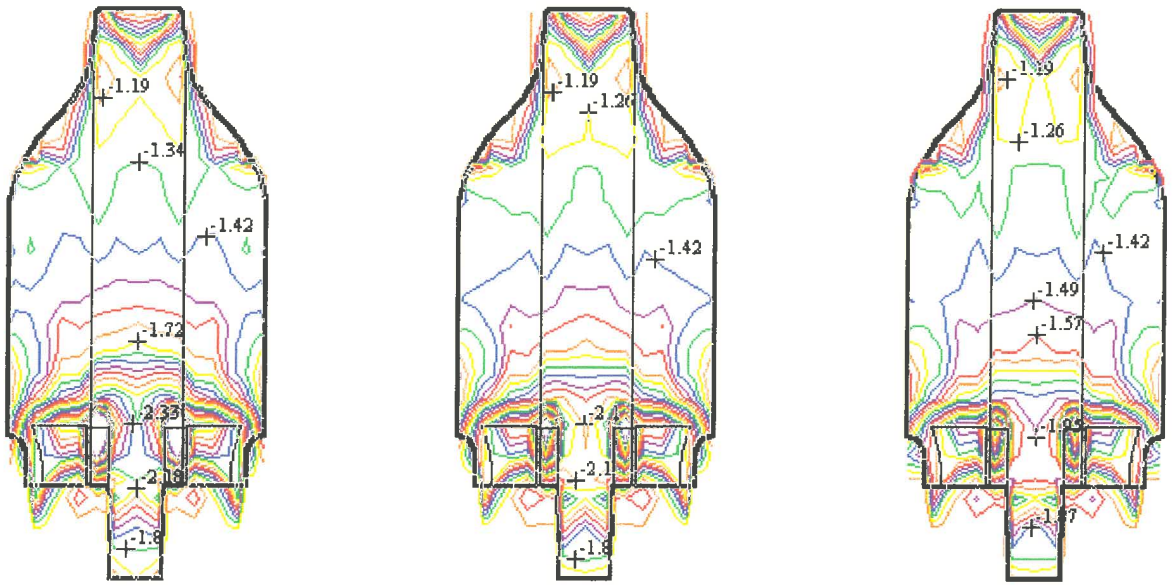

FRH=10; RRH=20 FRH=20; RRH=40 FRH=30; RRH=60

Figure 3-9 Pressure Coefficient contour maps of three Ride Heights

3.1.2.4 The Effect of Front-Flap Angle Adjustments

The front wing flaps, although fixed while driving, are the main mechanism used to balance the car aerodynamically. The flap angle of attack is therefore varied on a regular basis. As these devices deflect the air ahead of the floor, their influence was considered potentially significant and were therefore investigated next.

Two angles, one at 0° and the other at 26° were used for these tests. The two angles were the limits of the operating range of the flaps.

From Figure 3-10 it can be seen, that although changes in the contour lines are evident between the two cases, no dramatic variations are present. This suggests, that despite the influence on the shape of the pressure map, the level of downforce and the centre of pressure, that they were not the major contributors to the shape of the contours.

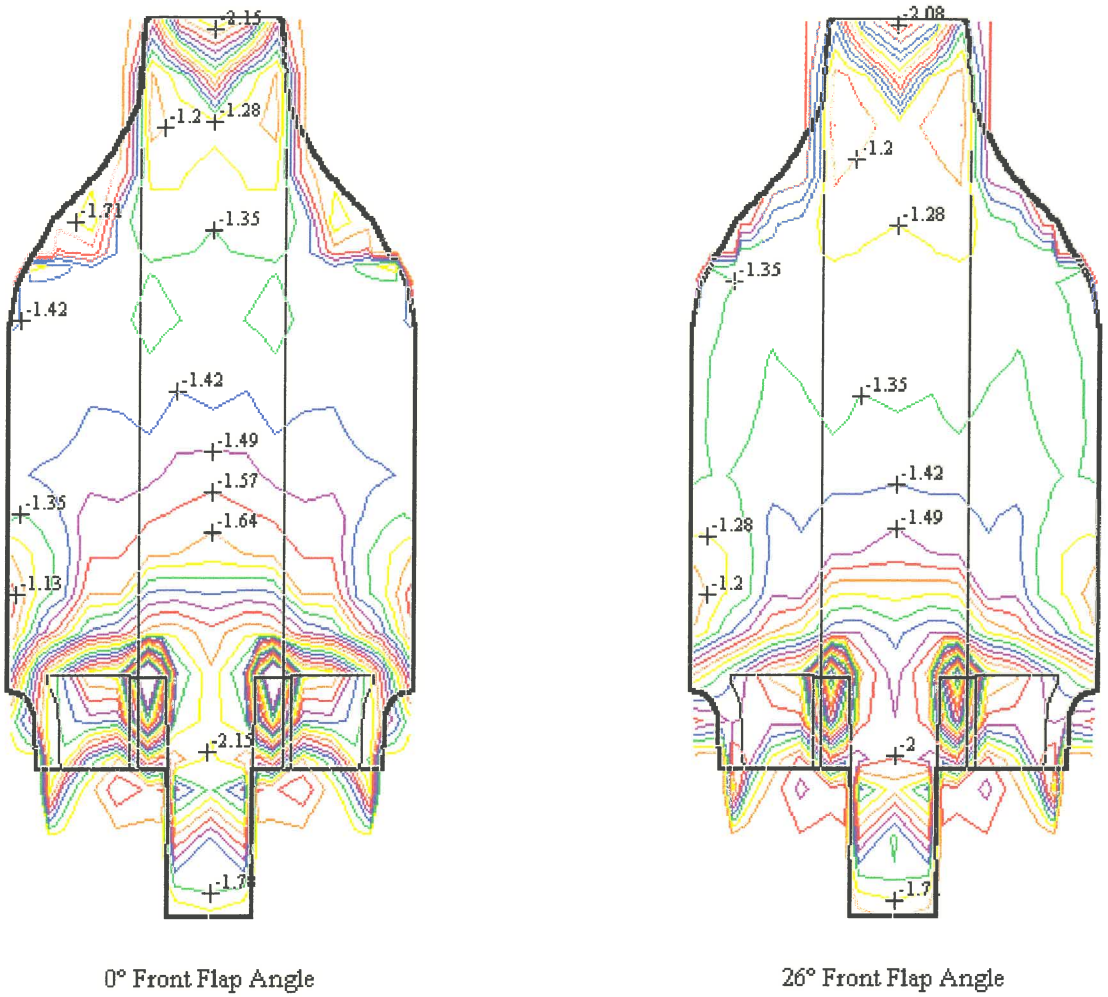

0° Front Flap Angle

26° Front Flap Angle

Figure 3-10 Flap Angle Comparisons

As the wheels are very prominent on Formula One cars, their effect was investigated next.

3.1.2.5 The Effect of the Wheels

The influence of the wheels were determined by removing them from the model. Figure 3-11 shows the pressure map of the floor in the absence of the wheels.

Comparing Figure 3-11 to the "wheels-on" case of Figure 3-7, it is clear that there are significant differences in the shape of the two maps. This is highlighted when the contour plots are compared as shown in Figure 3-12. The differences are visibly quantified by subtracting the wheels-off from the wheels-on case. This is plotted in Figure 3-13[xii].

[xii] The scale is adjusted so that the average of the difference lies on the ΔCp=0 plane. Surfaces above this plane therefore indicate the positive contributions of the wheels.

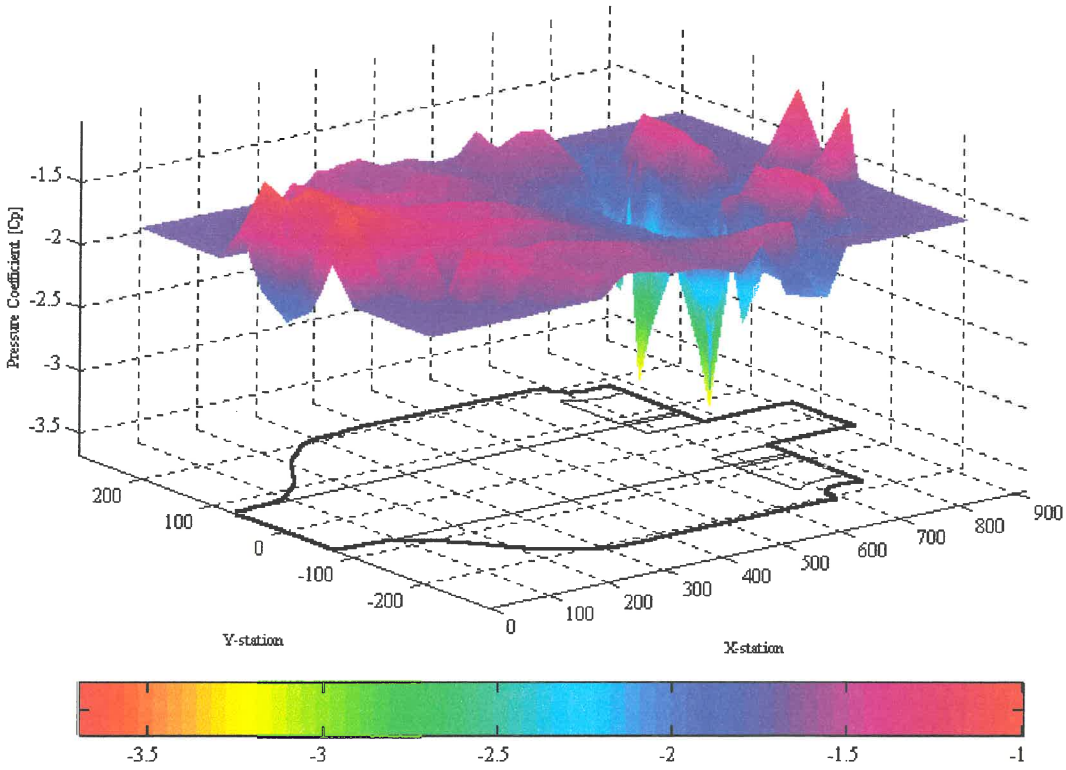

Figure 3-11 Pressure map of model floor with all 4 wheels removed

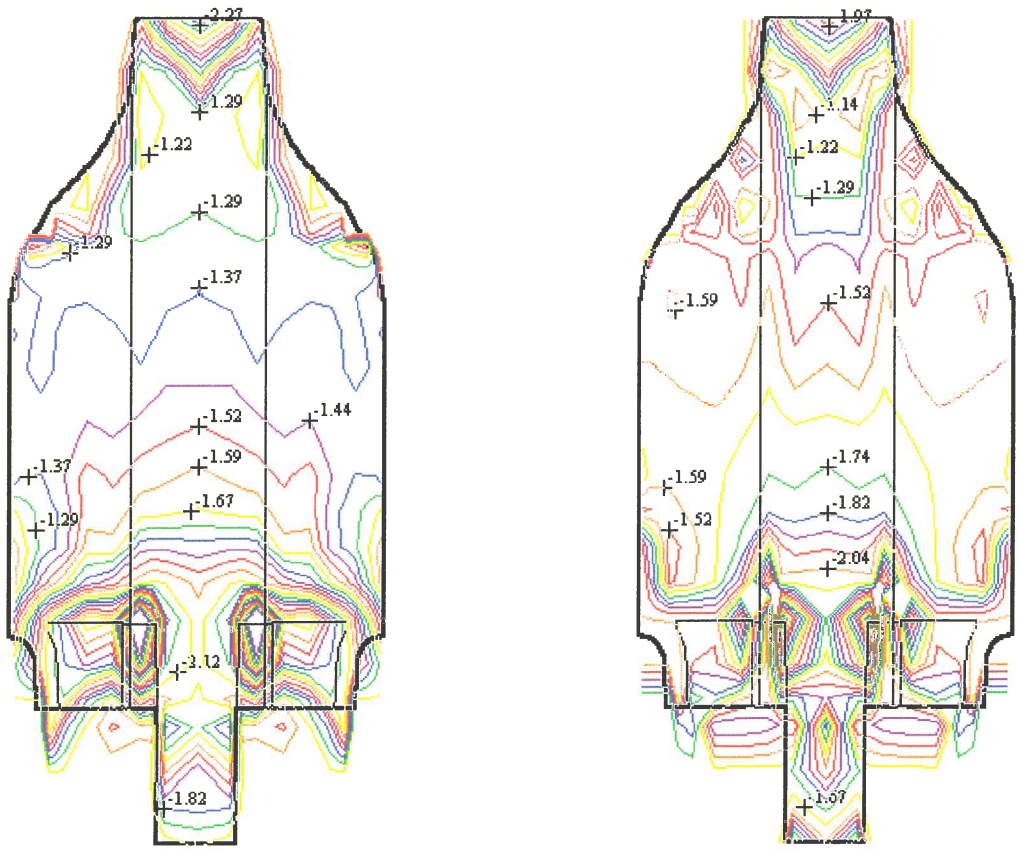

All Wheels On

All Wheels Off

Figure 3-12 Contour plot comparison of "wheel on" and "wheels off"

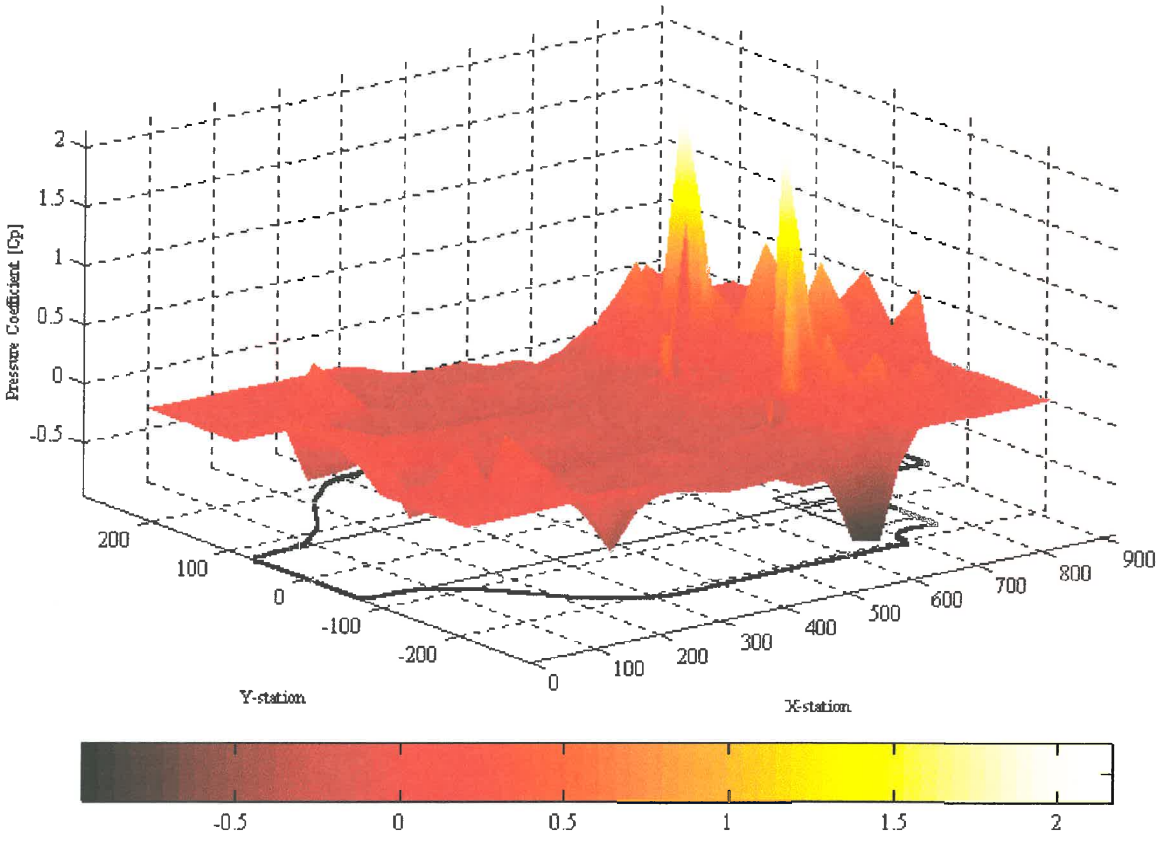

Figure 3-13 Differences between the "wheels on" and "wheels off" cases

By examining Figure 3-13 the changes in pressure distribution can be summarised as follows:

- Gains in downforce at the front splitter
- Losses in downforce around the circumference of the floor with two notable negative spikes. One immediately ahead of the rear wheels and the other by the air cooling intakes at the leading edge of the side-pods. A small positive spike is also visible just ahead of the cooling intakes.
- Distinct gains in the diffuser area
- A mild but extensive depression over the central floor area.

To understand the origin of these phenomena, two further tests were conducted. For the first test, the model was run without the front wheels, while the second test ran without the rear set. The results, as shown in Figure 3-14 and Figure 3-15 are plotted relative to the wheels-on case. The colour scale is identical to that of Figure 3-13.

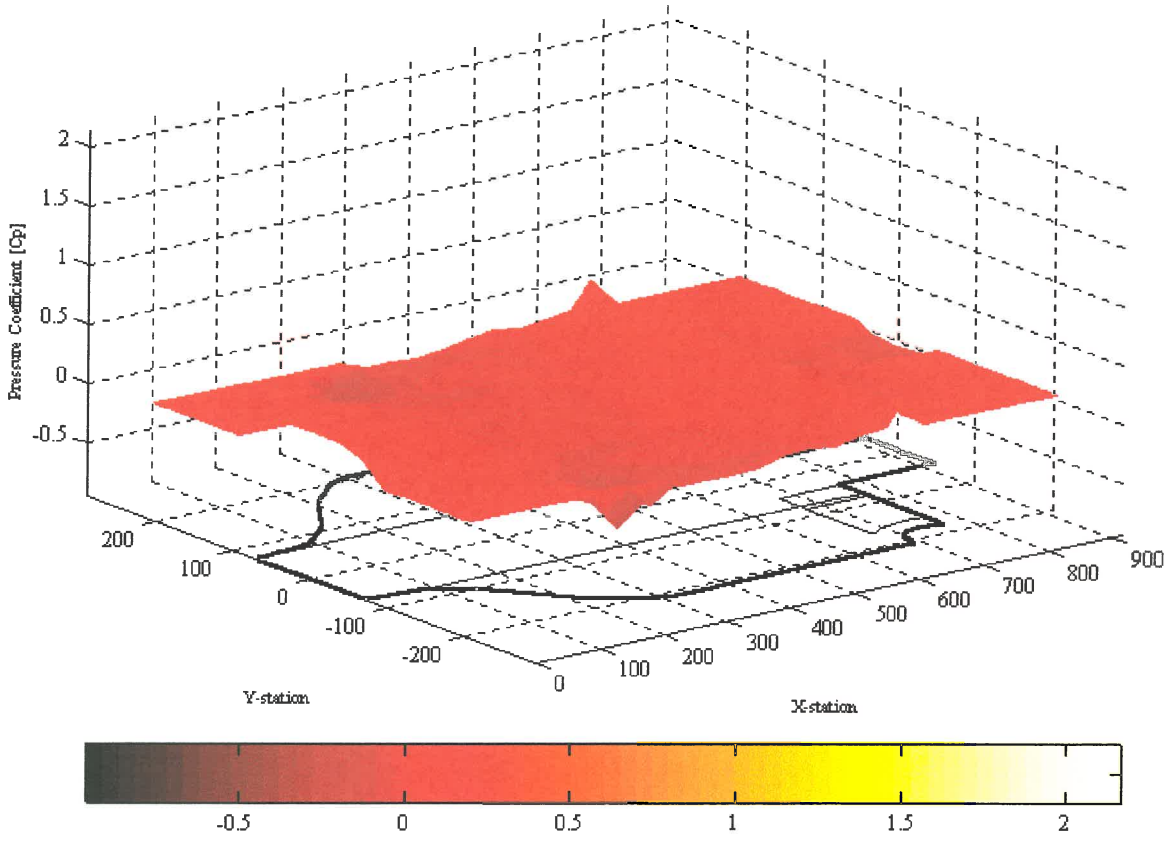

Figure 3-14 The relative effect of removing only the front wheel set

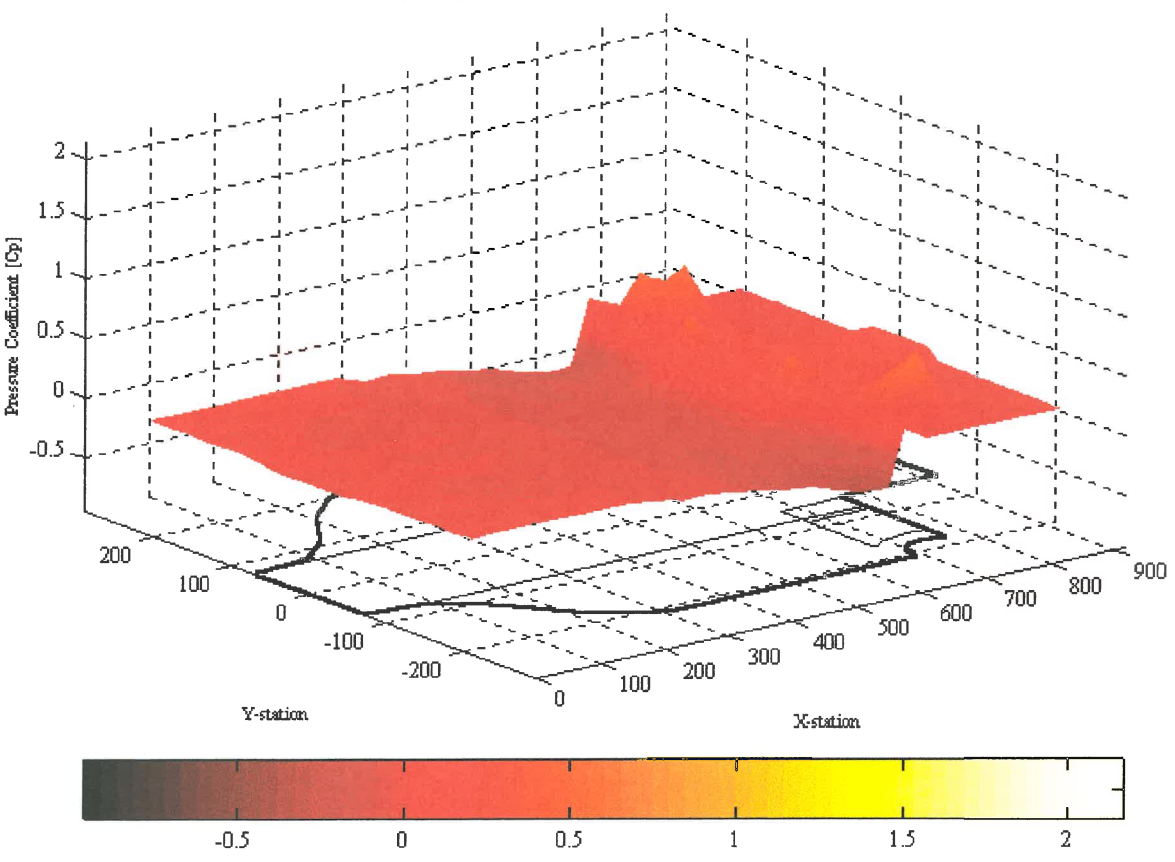

Figure 3-15 The relative effect of removing only the rear wheel set

Comparing Figure 3-14 and Figure 3-15 to Figure 3-13, it is evident that neither show changes as pronounced as when the model had no wheels. This seems to suggest that no set is uniquely responsible for the flow-field changes. This is confirmed when the wheel-set runs are compared to the wheel-off case, as shown in Figure 3-16 and Figure 3-17. From these figures, it seems that neither of the wheel sets dominate the flow field and only one of the sets is required to induce changes of the same magnitude as indicated in Figure 3-13. Therefore, when the flow field has been established by either set, the other only causes more subtle and generally more local changes in the pressure field.

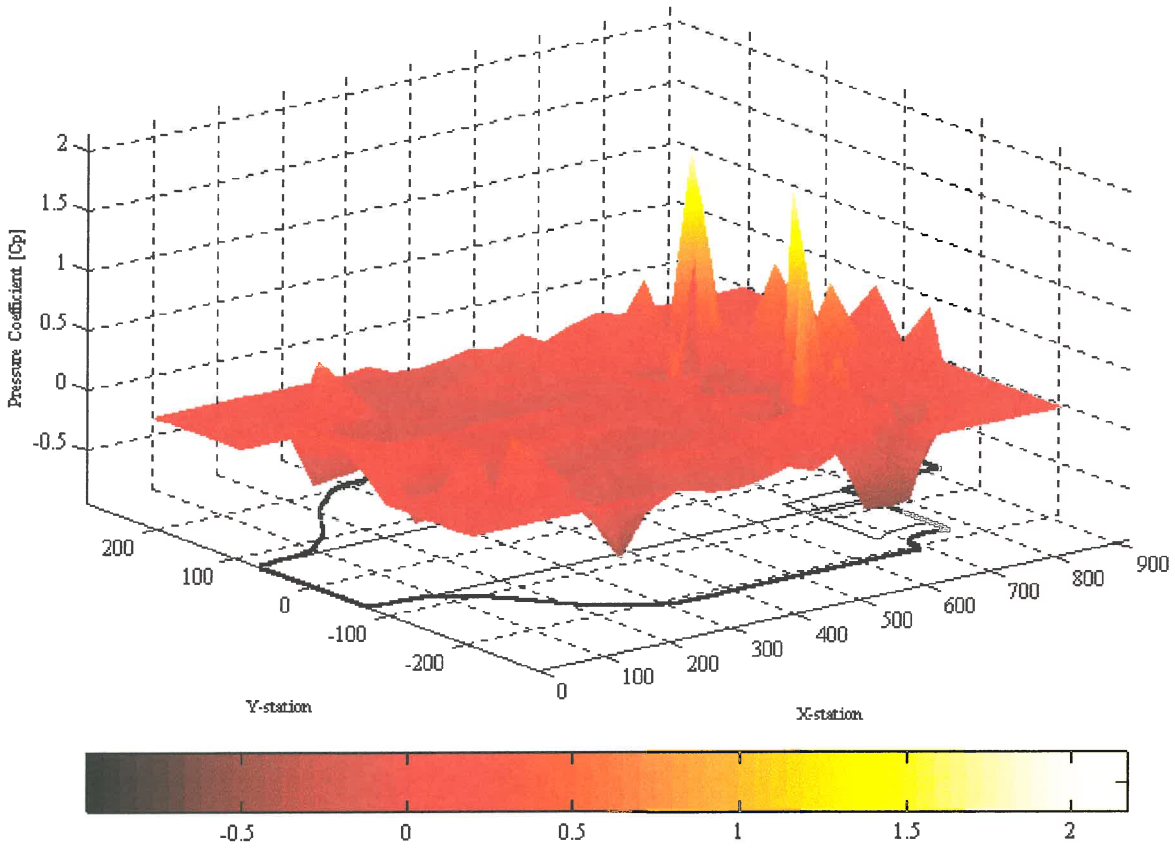

Figure 3-16 The relative effect of adding only the front wheel set

By examining the four figures presented above, it becomes possible to expand on the set of conclusions made earlier.

- The front wheels

The front wheels notably decrease the pressure at the front-splitter area. One way of explaining this, is to examine the vortices shed by the wheels[8]. The first set is shed at the contact patch of the tyres. The other is created by the interaction of the front wheels with the trailing edge of the front flap and the front-wing end-plates. These vortices were clearly visible when smoke flow visualisation was used. The symmetry of these vortices form a virtual nozzle around the centre line of the car. This creates an area for the oncoming air to accelerate through. The clockwise direction of these vortices also removes air from this channel, inducing a region of even lower pressure. The net effect is higher quality and higher velocity air under the floor. This effect can be seen to extend all the way to the rear diffuser.

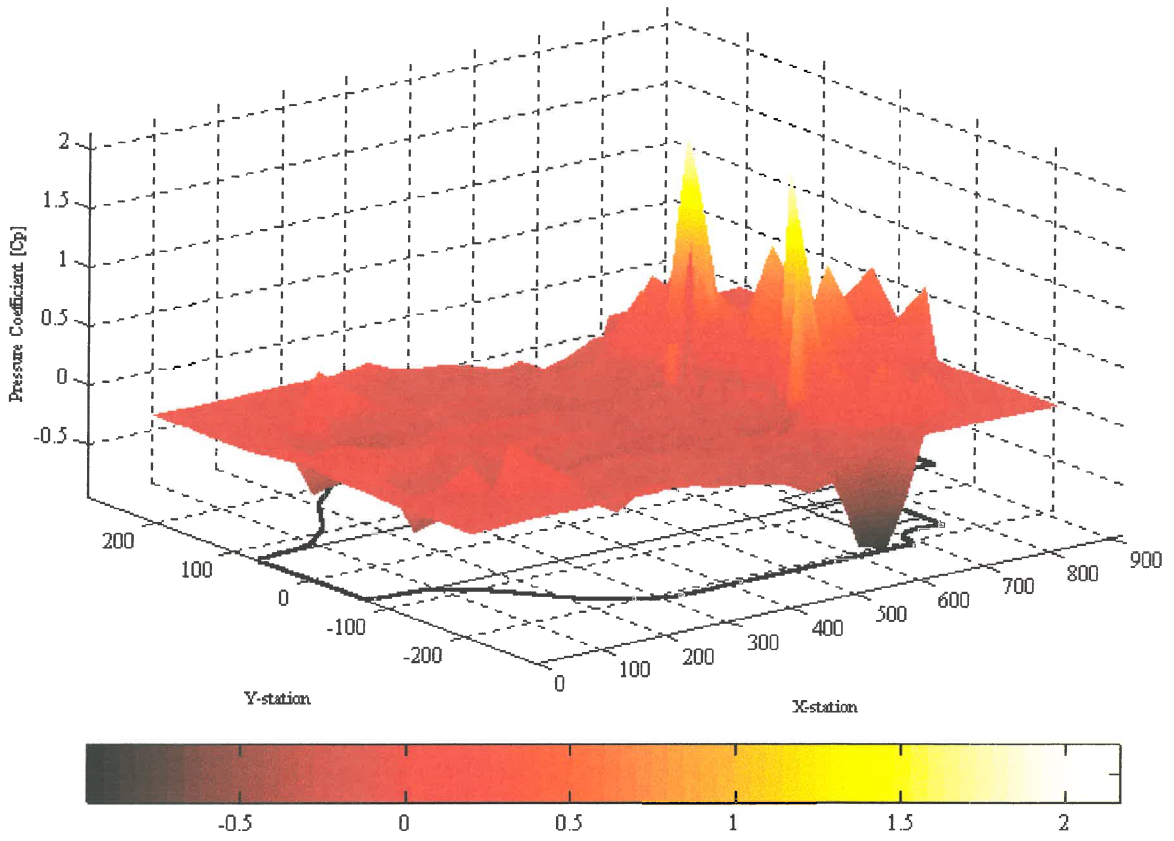

Figure 3-17 The relative effect of adding only the rear wheel set

The wake produced by the front wheels increases the amount of inflow at the edges of the floor. This effect is highlighted when the rear wheels are removed. Most notable are two spiky sets. One set at the outboard leading edge of the side-pods and the other set, at the floor-plate area of the rear diffuser. Here, the lower pressure induced by the front-wheel vortices under the floor, causes an influx of higher pressure air.

- The rear wheels

The stagnation point in front of the rear wheels induces a high pressure "bow wave". This area of higher pressure is quite extensive and in the absence of the front wheels, covers almost the entire floor area ahead of the wheels.

The vortices shed by the rear tyres on the in-board side, assist the diffuser by increasing the momentum of the flow in this area. The net effect is a decrease in the local static pressure.

To quantify these tests, the lift coefficients and the centre of pressures of the isolated floor was calculated for all four cases by surface integration as described by Equation 2-6 in section 2.2.2.2. The results are presented in Table 3-4. The COP is expressed as a percentage of the downforce available at the front wheels. For example:
If the COP was 0.7 x length of the wheelbase (WB) behind the front wheel centre line (20% behind the centre of the WB) 70% of the total downforce would be available at the rear wheels and therefore only 30% of the downforce would act on the front wheels (30%F).

From Table 3-4 it can be seen that the wheels have a negative effect on the downforce of the floor. The rear-wheel case produces the lowest level of downforce and moves the centre of pressure furthest to the rear.

Test Case	COP (%F)	Lift Coefficient ($-C_L$)
All wheels on	31.95	1.528
All wheels off	33.30	1.603
Only front wheels on	32.85	1.569
Only rear wheels on	31.85	1.502

Table 3-4 Lift Coefficients and balance of the wheel tests

Table 3-4 indicates that the wheels have a net negative effect on the downforce produced by the floor. It is possible to minimise their effect by using aerodynamic devices such as turning vanes or barge boards. It is potentially even feasible to use these devices to isolate the positive effects of the wheels and to improve the overall aerodynamic performance of the car.

The discussion in this section has been mainly centred around the effect of the wheels at off-centre line positions. To conclude this section, the effect of the wheels on the centre-line pressure distribution is examined by comparing the wheels-off case to the wheels-on case. The result of this comparison is shown in Figure 3-18.

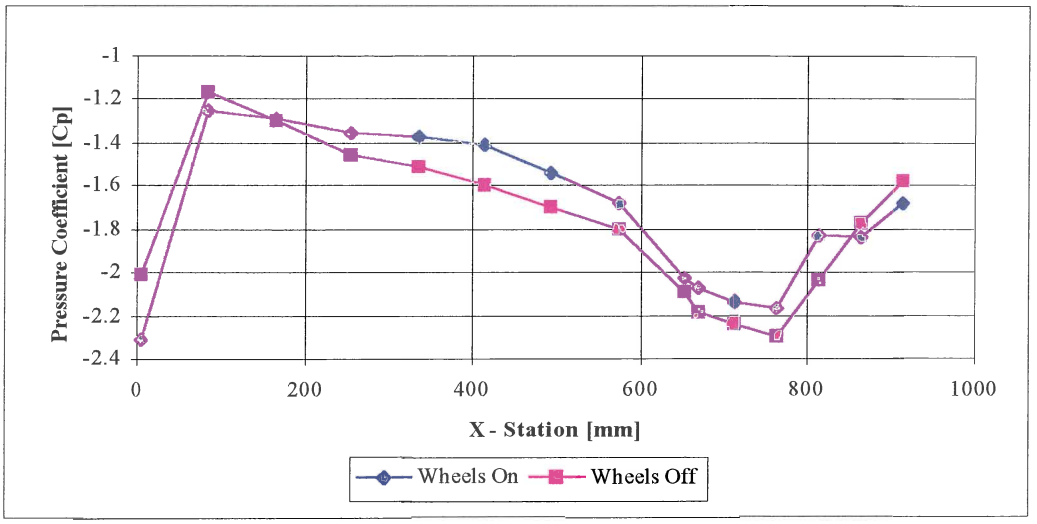

Figure 3-18 Centre-line pressure coefficient comparison: wheels-on vs. wheels-off.

From Figure 3-18 it can be seen that despite the significant influence of the wheels at positions away from the centre line, the effect of the wheels seems less influential in this area. This suggests that the fundamental shape of the centre-line pressure profile is not a function of the wheels.

3.2 Computational Investigation

Due to the close proximity of open-wheel racing cars to the ground, the interaction between the ground and the car becomes very important. This is often a major factor in the characterisation and understanding of the flow phenomena of these types of vehicles. Experimental studies therefore require rolling-road facilities to capture these phenomena. As an aid to this expensive and often very time-consuming method, CFD is being used by some

Formula One racing teams[9,10]. This is because the computer provides the designer with a virtual wind-tunnel environment where major changes can be performed with minimal cost implications. Due to the complexity and scale sizes of the flow, assumptions have to be made during the solution process. Numerical flow simulation therefore still needs to be correlated with experimental studies to verify the accuracy of the approximations and of the solution.

In this study CFD was used to investigate the air flow beneath the floor of the 30% scale model of the Forti Ford racing car. Two flow solvers were used to solve the full Reynolds-Averaged Navier-Stokes equations on a two-dimensional curvilinear grid. The first used Roe's flux-difference splitting algorithm, and the second was the SIMPLE algorithm of STAR-CD with a two-equation turbulence model. Even though a two-dimensional centre-plane geometry was simulated, the effect of the rotating wheels was incorporated using experimentally-correlated boundary conditions. This was considered feasible due to the reduced influence of the wheels on the centre-line flow pattern as shown in Figure 3-18. The experimental results discussed previously were used to verify the computational results. By independently varying front and rear-air gaps, the effect of ride-height configuration on the flow is discussed. Finally, the sensitivity of flow field on velocity variation was investigated.

3.2.1 Computational Set-up

3.2.1.1 Grid Generation

The 2D geometry was treated as an internal flow problem. The upper boundary was the 2D centre section of the car undertray as obtained from CAD data. The lower boundary was used to simulate the rolling road. The remaining two boundaries were treated as inflow and outflow boundaries.

The 2D centre-line grid was not complicated, so an efficient and inexpensive algebraic grid-generation procedure could be used. The algorithm was developed so that grid rendering was semi-automated for ride-height changes. The correct pitch, air gap and resulting grid was produced by simply defining the desired front and rear ride heights. The user also had control over the first and last spacing at the inlet and outlet boundaries as well as at the entrance to the diffuser. Vinokur[39] stretching as described in section 2.3.4.1, was used to control the spacing of the internal points. The blending function[40] as described in section 2.3.4.1 was used to ensure that grid lines were normal to the upper and lower boundaries. The user had to define the power of the blending function and the transition index for blending.

A typical grid used for the flow simulation is shown in Figure 3-19 and Figure 3-20. Note the clustering in the boundary layer and in the transition to the rear diffuser. This was to ensure proper resolution of expected high gradients in the flow.

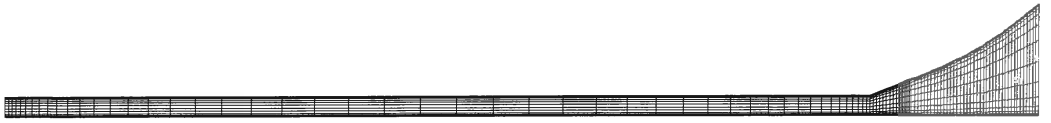

Figure 3-19 Typical 2D-grid: full-scale front ride-height = 40 mm; full-scale rear ride-height = 40 mm

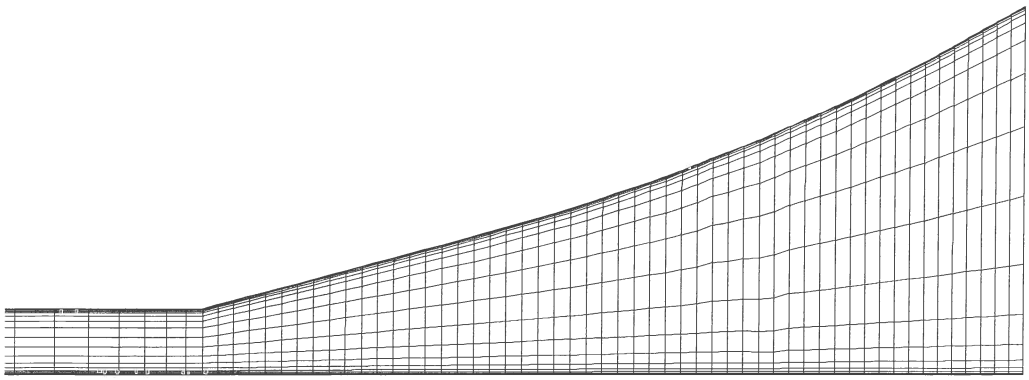

Figure 3-20 Close-up of diffuser section of grid

3.2.1.2 Flow Solvers

Two flow solvers were used during this study. These included an in-house laminar Reynolds-Averaged Navier-Stokes code, and the SIMPLE algorithm with k-ε turbulence model and wall function as implemented by STAR-CD.

The in-house code was based on Roe's flux difference splitting method as discussed in section 2.3.5.1 and in Appendix B.

3.2.1.3 Boundary Conditions

The Boundary conditions discussed in this section only apply to Roe's flux-difference splitting methods.

The inflow boundaries were specified using flow characteristics. As the flow to be solved was subsonic, only three relations were needed from the external flow at the inlet. The three relations were chosen as total pressure, total temperature and flow angle.

As the outflow conditions were subsonic and unknown away from the upper boundary, characteristic relations could only be used to solve three of the four characteristics. The final pressure characteristic, which needed to be specified from the exterior domain, was calculated using a line-iterative method as no information was available on the exterior flow field. Four different line-iterative methods as described by Wei[44], were used. The pressure on the floor at the diffuser exit was fixed using experimental data.

3.2.2 Computational Results

The flow conditions and dimensional parameters which were used are listed in Table 3-5.

All measurements were non-dimensionalised to pressure coefficients.

A typical runtime of the flow solver on an SGI Indy 133MHz workstation was 0.8msec/grid point/iteration. The maximum number of iterations used for a steady-state flow solution was 500 while a typical grid contained about 2500 points.

Parameter	Value/Description
Free stream velocity	24 - 100 m/s
Speed of rolling road	24 - 100 m/s
Temperature	295 K
Atmospheric pressure	101.325 kPa
Ratio of specific heats	1.4
Specific heat at constant volume	0.707 kJ/kgK
Viscosity	Sutherland's Law
Inflow angle	0°
Profile Length (MS)	0.92
FRH (FS)	10-40 mm
RRH (FS)	20-40 mm

Table 3-5 Flow conditions and Dimensional Parameters

3.2.3 Simulated Flow Field

Figure 3-21 and Figure 3-22 show the streamlines and relative pressure contours of two different ride-height configurations in the rear-diffuser area. Note the separation bubbles that formed against the undertray in the rear-diffuser area. These re-circulation bubbles were not observed experimentally. This can be ascribed to the interaction with the rear-wing assembly, which as described in 3.1.2.2, precludes the formation of these bubbles. The CFD rear boundary condition could not take the effect of the rear wings into account.

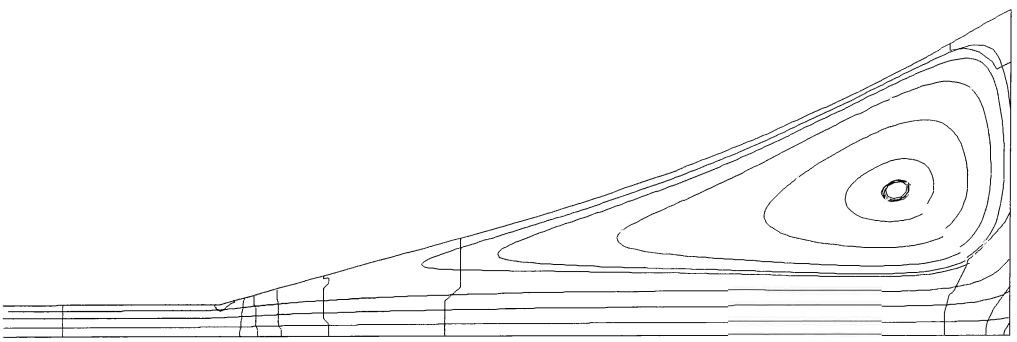

Figure 3-21 Streamlines and relative pressure contours in rear-diffuser area (FRH=10mm, RRH=20mm)

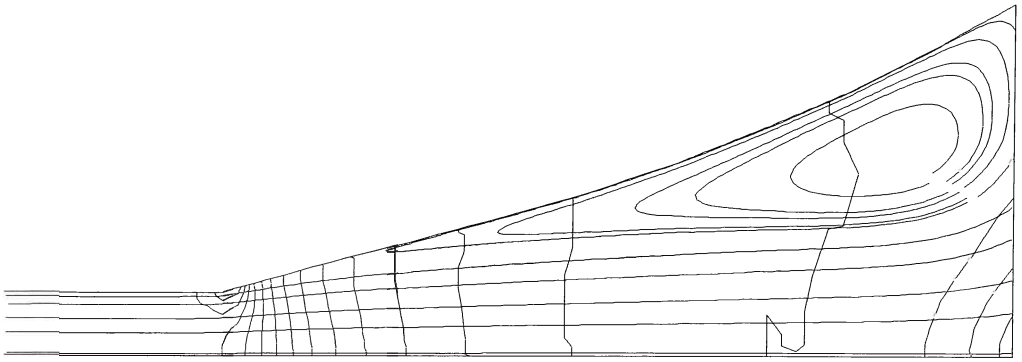

Figure 3-22 Streamlines and relative pressure contours in rear-diffuser area (FRH=40mm, RRH=40mm)

3.2.4 Variation of Road Speed

To illustrate the sensitivity of the solution to Reynolds-Number changes, the road and free-stream speeds were varied. Figure 3-23 shows the result in the form of the normalised lift coefficient of a series of CFD simulations for the 40-40 ride-height configuration. The downforce coefficient is shown to increase with road speed as expected, but a saturation point is reached.

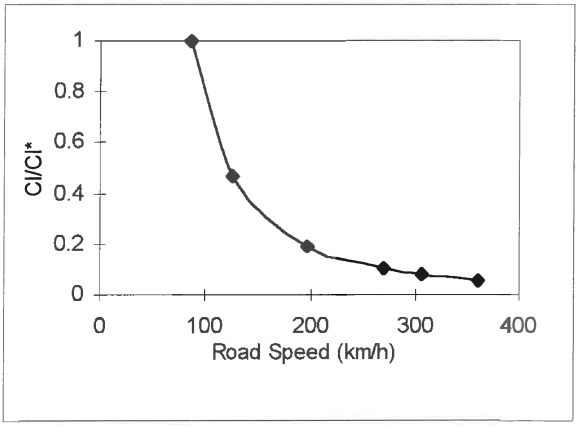

Figure 3-23 Normalised lift coefficient as a function of road speed (ride-height configuration 40-40)

3.3 Pressure Coefficient Correlation on the Centre Line

The centre-line pressure coefficients for five different computations are compared to wind-tunnel data in Figure 3-24. The data shown are for FRH = 40mm and RRH = 40mm. It can be seen that runs a and b are shifted upwards when compared to the wind-tunnel results (f). This is because the solutions generated using STAR-CD are relative to a user-specified reference pressure. After the reference pressure is adjusted to coincide with the experimental data, a better correlation is obtained (d and e). This adjustment is not necessary for the RANS in-house code (c), as pressures are calculated as absolute. The large spike obtained from this run is due to the sharp discontinuity present in the modelling of the transition from the flat undertray to the diffuser. The spike can be reduced by introducing a more even transition in the grid. The differences between runs a and b (and d and e) clearly illustrate the effect of turbulence on the solution.

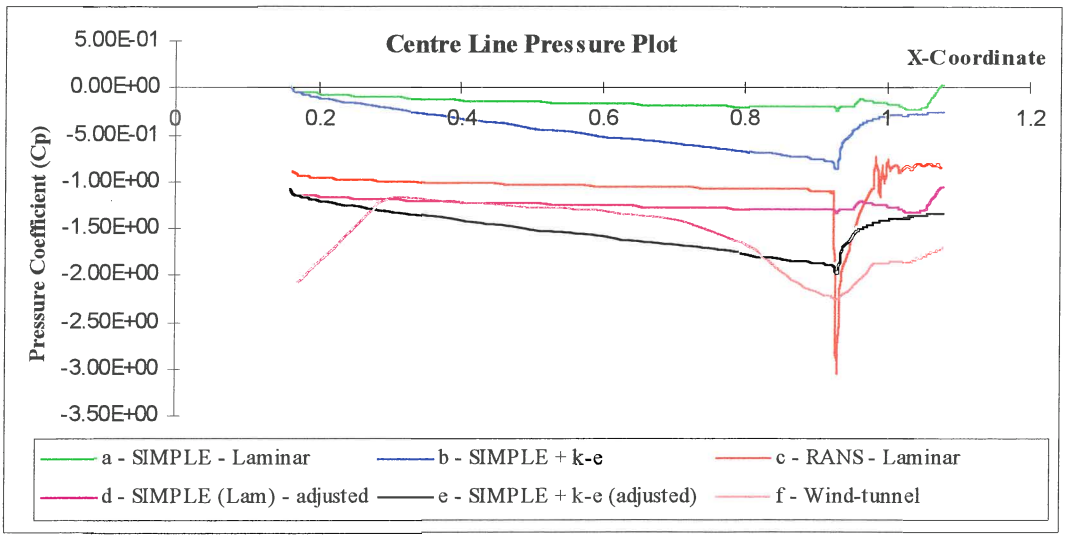

Figure 3-24 Centre-line pressure plot correlation

It is evident from the data that there are two distinct areas where the correlation between the wind tunnel and the CFD data is not accurate. These are, firstly, the area at the entrance to the under-body and, secondly, the exit- diffuser area. At the entrance area the correlation is poor because the 3D acceleration of the air due to the interaction between the front splitter plate and chassis, could not be simulated with the under-tray in isolation. At the exit, the deviation is probably caused by the omission of the rear-wing assembly.

3.4 Conclusion

In this investigation, the Parmalat Forti Ford FG01-95 racing car was used to study the flow beneath the floor of a Formula One car. The study was conducted using experimental and numerical techniques. The numerical part was, in an attempt to find more efficient development techniques, directed towards the use of centre-line geometry in predicting the flow-field trends. The experimental leg was aimed at establishing the aerodynamic influence of components external to the floor. As the numerical component used experimental data for verification, the wind-tunnel study was presented first.

The experimental study consisted of building a 30% scale model and testing it in a rolling-road wind tunnel. To capture the flow field beneath the floor, the model was fitted with 92 static-surface pressure ports.

The investigation revealed, that despite the obvious dependency of the pressure distribution on the geometry of the floor, front-flap angle and ride-height adjustments had comparatively little effect on the shape of the pressure contours. The wheels however, had a dominating influence on the shape of the pressure map. Despite the fact that the rear wheels had the biggest effect on the aerodynamic coefficients, the front wheels played an equal and independent role in setting up the underlying flow pattern beneath the car. It was however, also shown that the classic floor-pressure profile, characteristic to smooth-bottomed racing cars with front splitters and rear diffusers was still clearly visible even after the wheels had been removed.

It was suggested that the potential exists to minimise and overturn the detrimental effect of the wheels by using add-on devices such as barge boards and diffuser turning vanes.

The numerical investigation used two flow solvers to solve the full Reynolds-Averaged Navier-Stokes equations on a two-dimensional curvilinear grid. Roe's flux-difference splitting algorithm, and the commercial package, STAR-CD with a two-equation turbulence model was used. The 3D nature of the flow field was imposed on the centre-line simulation by partially using experimentally-correlated boundary conditions. It was found that although the flow phenomena beneath the isolated floor could be predicted and variations in ride height produced the correct trends, the absence of the rest of the vehicle lead to premature separation in the diffuser. The effect of the front splitter could also not be predicted. Reynolds-Number independence with respect to the lift coefficient was also demonstrated.

To investigate the attainable correlation between the numerical and experimental flow around a racing car, a new study was launched where a less complicated experimental model was used. This is the topic of the next chapter.

4. THE FLOW AROUND A GENERIC BMW TOURING CAR

The aerodynamic investigation of the Parmalat Forti Ford F1 racing car, as presented in Chapter 3, highlighted the difficulties in correlating the numerical centre-line simulation of the isolated floor to the experimental 3D case. The effects of components such as the rear wing and front splitter could not be imposed on the numerical model by simply using experimentally-measured boundary conditions. The conclusion was reached that correlation could potentially be improved by including more detail in the simulation. To address this problem effectively on a 2D basis, the complete centre-line of the car had to be simulated.

The computational costs involved in simulating the complicated F1 profile made this approach very expensive. A less complicated model was therefore chosen. A generic model of a $1/12^{th}$ scale closed-wheel BMW Touring Car was used to investigate the accuracy of centre-line simulations. The smaller scale, as compared to the F1 study, offered the following advantages:

- Lower model-manufacturing costs.
- A smaller and less complicated numerical grid.
- Increased numerical efficiency.
- Reduced tunnel size and related operating costs.

Although the smaller scale resulted in a loss of detail, the scale was still big enough to ensure a representative racing car. Furthermore, full-scale correlation was not the intention of this study and so the loss in detail would not affect the correlation exercise.

A closed-wheel vehicle was chosen to limit the effect and influence of the wheels. The generic nature of the model ensured that a smoothed-bottomed floor could be used and guaranteed the presence of components such as the front splitter and rear diffuser. The choice of motor manufacturer was based on the availability of moulds in the form of commercial scale-model electric-toy racing cars. The body shells of these "toys" offered sufficient detail and eliminated the need for the manufacturing of expensive and complicated moulds.

This investigation, similar to the one presented in Chapter 3, also consisted of an experimental and a numerical study. In this case however, the emphasis was placed on the numerical simulations. The experimental side was mainly used to determine a baseline set of results for use in the computational investigation.

The experimental data was obtained by constructing a scale model of the BMW, fitting it with static-surface pressure taps and testing the model in a wind tunnel. After repeatability and Reynolds-Number independence are demonstrated, the discussion of the experimental results is introduced by examining the similarities between the under-body flow of the BMW and the Parmalat Forti Ford. The baseline experimental results for use in the numerical part is then presented. Included in this section, is a discussion on the interaction between a rear-mounted aerodynamic device and the under-body flow of the BMW. These results are used to explain the underlying phenomena responsible for rear-wing downforce on a sedan-based racing car.

The computational flow solver and grid-rendering software of STAR-CD was used in the numerical investigation. After a description of the grid, the effect of three different turbulence models is investigated. From this study it is seen that although similarities between the experimental and numerical cases exist in certain areas, the correlation under the floor is still

poor. It is concluded that the most likely cause of these discrepancies lies within the computational methodology. At this point it was decided to terminate this study with a proposed outline of work which should be included in a future investigation to improve the numerical accuracy. This discussion includes further simulations and related conclusions. The effects of mesh density and the dependency on the choice of turbulence model and related parameters are covered.

4.1 Experimental Investigation

4.1.1 Experimental Set-up

The closed-return LSWT at the University of Pretoria, South Africa was used for the experimental tests. The wind tunnel had a 0.9x1.1x2m closed test section with a stationary floor. The six-component tail-sting strain-gauge force balance of the tunnel was not used.

To avoid tunnel boundary-layer problems a raised platform was installed. The platform had a knife-edge profile at the leading edge and was approximately 150 mm above the tunnel floor. The platform was inclined at a slight negative angle to limit the development of the platform boundary layer[14] as described in section 2.2.1.2.

The effective tunnel blockage was calculated to be approximately 3% for the $1/12^{th}$ scale model of the Generic BMW German Touring car. Blockage calculations were referenced to the raised platform.

The tunnel tests were performed at velocities ranging from 40 to 60 m/s. Using the length of the model as the characteristic length, the Reynolds Numbers were in the range of $1x10^6$ to $1.7x10^6$. This was above the critical Reynolds Number as discussed in section 2.2.3.1.

The nose of the model was mounted 360 mm from the leading edge of the platform and the rear end of the vehicle was 675 mm in front of the trailing edge of the platform. The trailing-edge distance was chosen to exceed Garry's[15] criteria for drag errors as described in section 2.2.1.2.

The mould used to construct the model was the body shell of a $1/12^{th}$ scale electric racing car model. The upper shell was constructed using glass fibre. The model had a smooth wooden floor with closed wheel arches. The engine cavity was closed off by extending the floor from the leading edge to the trailing edge of the model. The scale wheels, which were taken from the electric racing car, were mounted onto the test platform ensuring, as required by Cogotti[46], zero air gap between the platform and the wheels. The wheels were fixed and were therefore not free to rotate.

The upper and lower centre-line surface of the model was fitted with 38 centre-line pressure ports as shown in Figure 4-1. All pressures were corrected using the continuity-based blockage-correction factor as proposed by Sykes[47] and discussed in section 2.2.3.2.

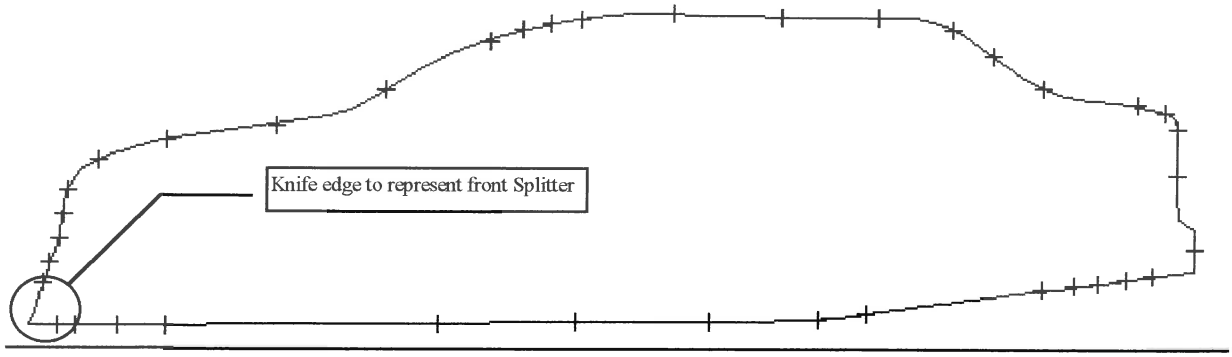

Figure 4-1 Centre line profile showing the positions of the pressure tapping

From Figure 4-1 it can be seen that the front splitter is represented by a knife edge. The inclusion of a rear diffuser is also clearly visible.

The pressure taps were connected to a Scanivalve and data-acquisition system. The valve was mounted inside the model to limit the cabling to and from the model. Cables leaving the model were taken out behind one of the rear wheels. The schematic representation of the model as mounted in the wind tunnel is shown in Figure 4-2.

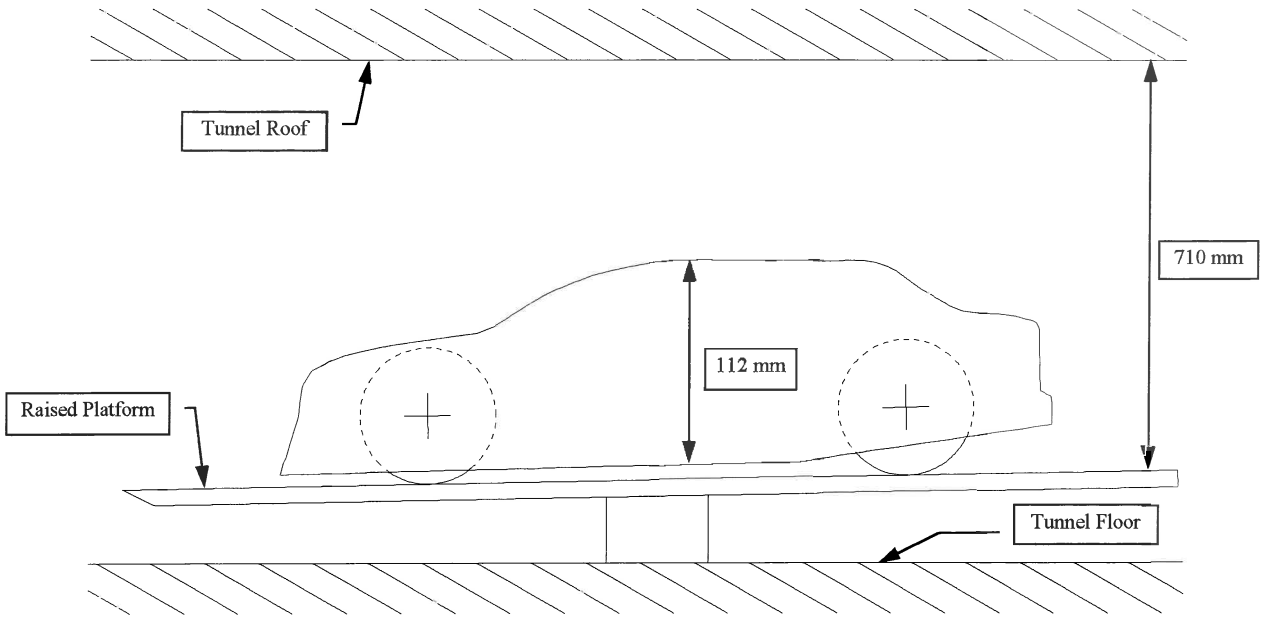

Figure 4-2 Schematic layout of the BMW model as mounted in the wind tunnel

4.1.2 Experimental Results

4.1.2.1 Repeatability

The repeatability of two identical runs, made on different days is summarised in Table 4-1. All the pressure taps were used for the calculations.

Variable calculated	Result
Mean Pressure coefficient of Run 1 (C_P)	-0.1241
Mean Pressure coefficient of Run 2 (C_P)	-0.1252
Mean difference between Runs	0.0020
Mean difference expressed as a percentage (%)	1.3

Table 4-1 Results of repeatability calculations

Differences of less than 1.3% will be interpreted as repeatability errors and not as aerodynamic changes.

4.1.2.2 Reynolds-Number Sensitivity

The success of CFD models in simulating the flow field around a car is very sensitive to the ability to predict the point or line of flow separation accurately. In a similar way, the aerodynamic coefficients and related pressures of experimental tests are also subject to separation and to the levels of turbulence in the boundary layer and in regions of separated flow. As explained in section 2.2.3.1, turbulence and separation can be represented at scale by ensuring Reynolds-Number independence. To ensure this, pressure readings were measured on the scale model at Reynolds Numbers ranging from $1.15x10^6$ to $1.73x10^6$. The results, as presented in Figure 4-3, were reduced to velocity comparisons as all the other parameters defining the Reynolds Numbers remained fixed.

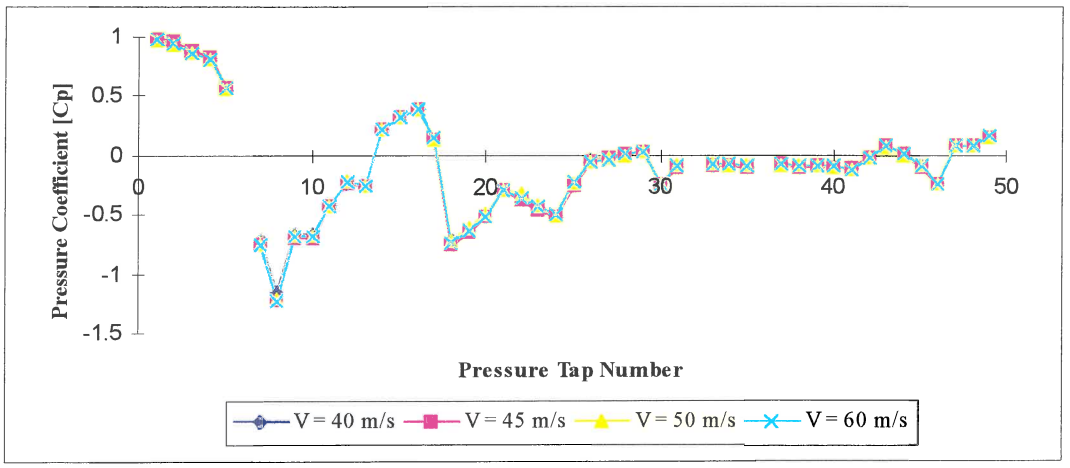

Figure 4-3 - Reynolds-Number Sensitivity

From Figure 4-3 it can be seen that there is almost no variation in the magnitude of the pressure coefficients. A test velocity of 40 m/s was therefore adequate to ensure Reynolds-Number independence. As these results are in good agreement with the findings of Barnard[16] who suggested a Reynolds Number in excess of $9.6x10^5$, all experimental tests and numerical simulations were performed at this speed.

4.1.2.3 The Characteristic Floor Pressures

To establish continuity with the F1 case study, the BMW floor-pressure coefficients were compared to the Forti coefficients. The results are displayed in Figure 4-4. The F1 data is identical to the values used in Figure 3-6.

As seen from Figure 4-4, the characteristic pressure drop at the front splitter and rear diffuser is also visible for the BMW. The pressure drop induced by the rear diffuser of the BMW is however, less pronounced than that of the Forti. This is to be expected as F1 cars are designed

to be aerodynamically superior, they run at lower FS ride heights, they have more complicated diffusers which run at higher angles and they carry a multitude of efficient wings. The higher aerodynamic forces generated by F1 cars are clearly indicated by the significantly lower pressure coefficients.

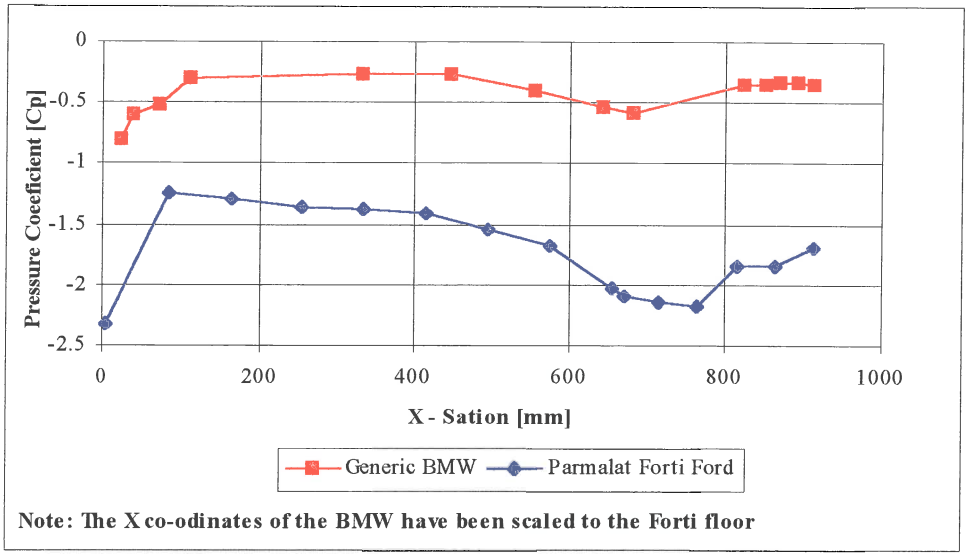

Figure 4-4 Under-body pressures of the Generic BMW and the Parmalat Forti Ford

Continuity with the F1 study has therefore been established.

4.1.2.4 The Centre-Line Pressure Distribution

The main aim of the experimental investigation was to provide a set of base-line results to which the CFD simulations could be compared. The results of these measurements are presented in Figure 4-5 to Figure 4-8 in the form of non-dimensional pressure coefficients. Each figure was chosen to represent a distinct physical region of the vehicle. These were defined to facilitate viewing and discussion. The regions were defined as:

- The nose area - Figure 4-5
- The upper surface area - Figure 4-6
- The rear area - Figure 4-7
- The floor area - Figure 4-8

X=0 and Z=0 are taken to be at the bottom leading edge of the car. All co-ordinates are given in model scale. These conventions are followed throughout the remainder of this chapter.

The lack of numerical correlation in the F1 case study, was amongst other reasons, attributed to the influential effect of the rear-wing assembly. The importance of this interaction was illustrated by placing a 20 mm vertical spoiler or Gurney flap (GF) on the small-scale BMW model. The GF spanned the entire trailing edge of the boot-lid. The results of this set-up were also plotted in Figure 4-5 to Figure 4-8.

It should be noted that the measurements presented in the four figures were made at discrete locations and the data points have simply been connected to establish trends and facilitate interpretation.

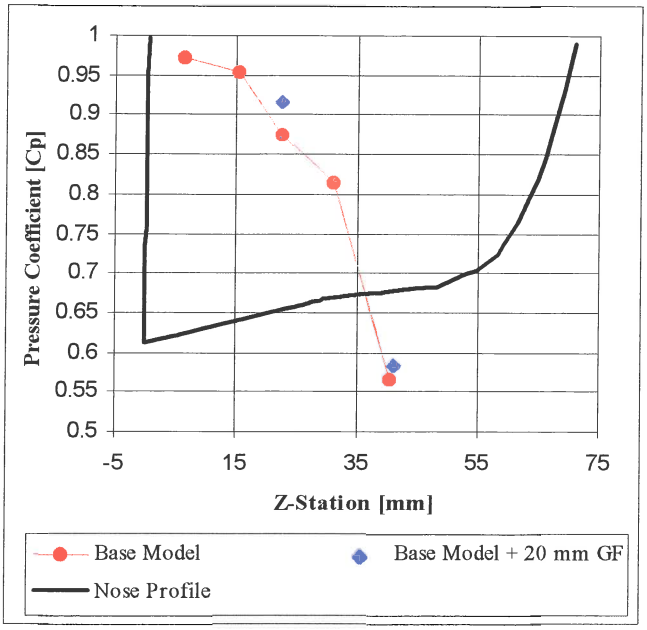

Figure 4-5 Pressure distribution on the centre line of the nose of the car[xiii]

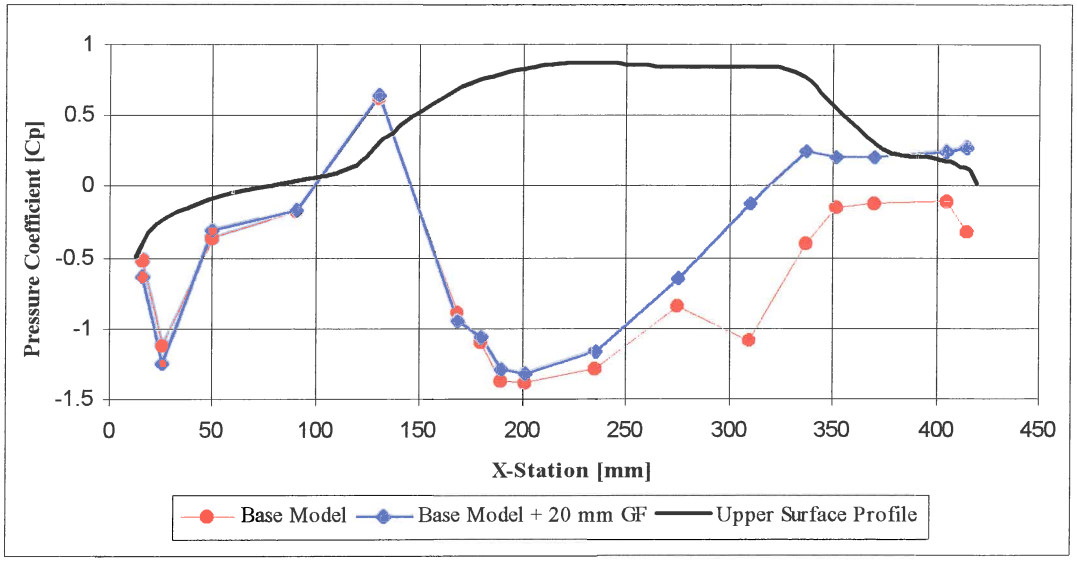

Figure 4-6 Pressure distribution for two tunnel runs on the centre line of the top of the car

[xiii] The "Base model + 20 mm GF" case only show the results of two pressure measurements. Three of the five ports became blocked during this run and were therefore not included.

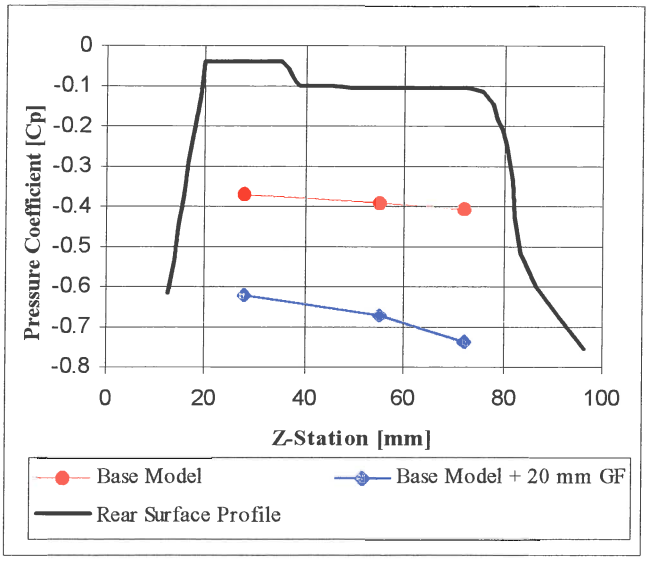

Figure 4-7 Pressure distribution for two tunnel runs on the centre line at the rear of the car

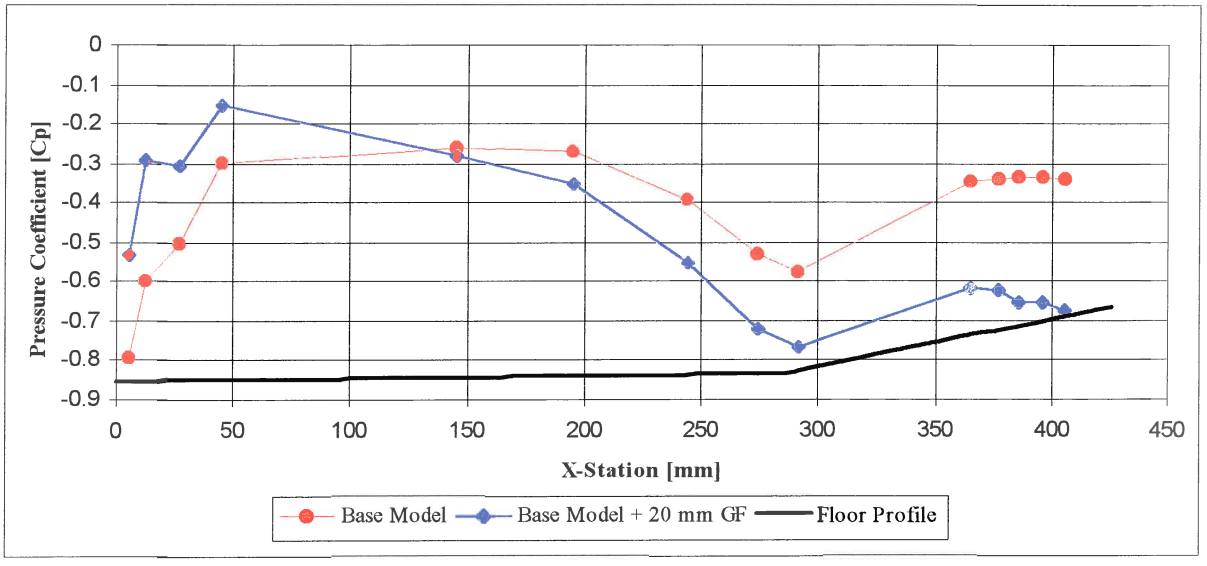

Figure 4-8 Pressure distribution for two tunnel runs on the centre line under the floor of the car

It is evident from the figures that the GF has a marked effect on the pressure distribution over most of the car. The pumping effect of this "wing" as described in section 3.1.2.2, can clearly be seen in Figure 4-8. It can be seen that for the GF case, the pressure under most of the floor was significantly lower than for the baseline case.

Examination of Figure 4-6 and Figure 4-8 also reveals the mechanism responsible for producing rear downforce on sedan-based racing cars fitted with boot spoilers or wings. In addition to the reduction in the under-floor pressure, the rear "wing" also increases the pressure over most of the aft section of the upper surface of the vehicle. The net effect is an increase in the pressure differential between the two surfaces. Rear downforce is therefore generated. Unfortunately, in this case, the increase in rear downforce is offset by a decrease in the front downforce. This is because the rear spoiler increases the pressure under the nose but the pressure on the upper surface remains almost unchanged.

The spoiler also increases the drag of the car. This effect, although not calculated, is evident from the lower base drag in Figure 4-7 and the comparatively insignificant change to the pressures at the front of the car as shown in Figure 4-4.

it can further be seen that although the GF changes the distribution of the pressures under the floor, the characteristic centre-line pressure profile, as discussed in section 3.1.2.2, remains unaltered.

4.2 Computational Investigation

The aim of this investigation was to extend the numerical study presented in section 3.2 by investigating the accuracy with which the centre line of a closed-wheel racing car could be approximated by a two-dimensional computational simulation. These results are presented in this section.

4.2.1 Computational Set-up

The computational domain used to solve the flow around the centre-line profile of the experimental 1/12th scale BMW was generated using a CAD system and PRO-STAR, the structured grid rendering pre-processor of STAR-CD. The grid was generated using a number of grid blocks which were matched to ensure connectivity. This approach was required to ensure an accurate centre-line profile and also to facilitate grid clustering in regions where high flow gradients were expected. To ensure a self-contained solution the grid was extended by three car lengths to the front, five car lengths to the rear and four car heights above the vehicle. The resulting grid as shown in Figure 4-9 contained 24240 cells.

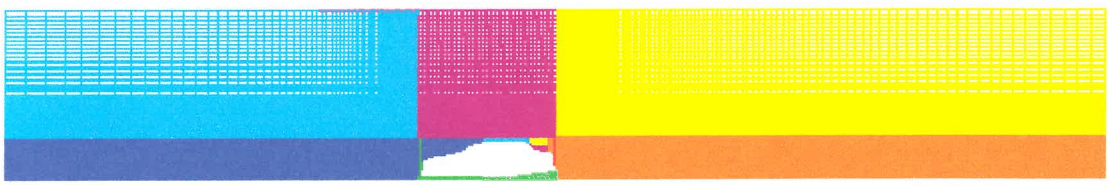

Figure 4-9 Centre-line grid for the 1/12th scale Generic BMW

The spacing between grid-cell centroids on the surface of the vehicle is described in Table 4-2.

	Average Spacing [mm]	Minimum Spacing [mm]	Maximum Spacing [mm]
The Nose	4.83	2.99	5.46
The Upper Surface	7.82	1.16	10.37
The Rear	2.93	0.811	3.84
The Floor	8.52	8.23	8.67

Table 4-2 Grid spacing on the surface of the BMW

The SIMPLE algorithm as implemented by STAR-CD was used in this investigation. This method was considered more suitable than the PISO and SIMPISO STAR algorithms as the flow was assumed to be steady and excessive grid skewness could be avoided during meshing.

The boundary and flow conditions which were used to close off the system of numerical equations are summarised in Table 4-3 and Table 4-4.

Boundary Description	Boundary Position	STAR Boundary Condition
Inlet	Far field - 3 car lengths in front	Free stream horizontal velocity
Outlet	Far field - 5 car lengths behind	Percentage mass Flow
Solid 1	Vehicle Body	Solid
Solid 2	Road	Solid
Reflection	Far field - 4 car heights above	Reflection
Centre Line	Either side of "1 cell thick" grid	2D Symmetry

Table 4-3 Boundary conditions

Flow Condition or Dimensional Parameter	Specification
Free-stream velocity	120-150 km/h
Density of air (constant)	1.205 kg/m^3
Temperature of the air	295 K
Atmospheric pressure	101.325 kPa
Ratio of specific heats	1.4
Specific heat at constant volume	0.707 kJ/kgK
Viscosity	Sutherlands Law
Turbulence mixing length	0.01
Turbulence intensity	0.1

Table 4-4 Flow conditions and dimensional parameters

4.2.2 Computational Results

The regions of separated flow and related turbulence around a racing car suggests that turbulence models would have a significant role to play in achieving correlation. The effect of turbulence models was therefore investigated first to obtain an indication of potential correlation.

4.2.2.1 The Effect of Turbulence Models

The three standard STAR-CD turbulence models for high Reynolds-Number flows were used to investigate the effect of turbulence on the solution. For comparative reasons a laminar solution (no turbulence model) was also generated. The numerical solutions that are discussed in this section were categorised according to the turbulence model that was employed. The four solutions are described as:

- The laminar flow case (No Turb)
- The standard k-ε turbulence model flow case (KE)
- The k-ε RNG turbulence model flow case (KE-RNG)
- The k-ε turbulence model of Chen flow case (KE-Chen)

The bracketed abbreviations are used to describe the results in the figures which follow.

The numerical solutions were all compared to the experimentally measured data as discussed in section 4.1.2.3.

The results of the four turbulence solutions are presented in Figure 4-10 to Figure 4-13 in similar fashion to the figures of section 4.1.2.4.

From Figure 4-10 it can be seen that there is agreement between the experimental data and the laminar flow case in the upper region of the front nose area of the car. The deviations near the ground are caused by the incorrect prediction of the magnitude and position of the stagnation point. The higher physical position of the numerically-calculated stagnation point implies an incorrect split of the flow around the vehicle. This has implications downstream as the volume of air available to perform work above and below the car will be incorrect. All three turbulence models suffered with this inaccuracy. Of the three turbulence models, the standard k-ε model is seen to perform the worst. This model seems to predict a relatively large stagnation area. The RNG and Chen models, although conservative, approach the experimental pressure contour with higher accuracy.

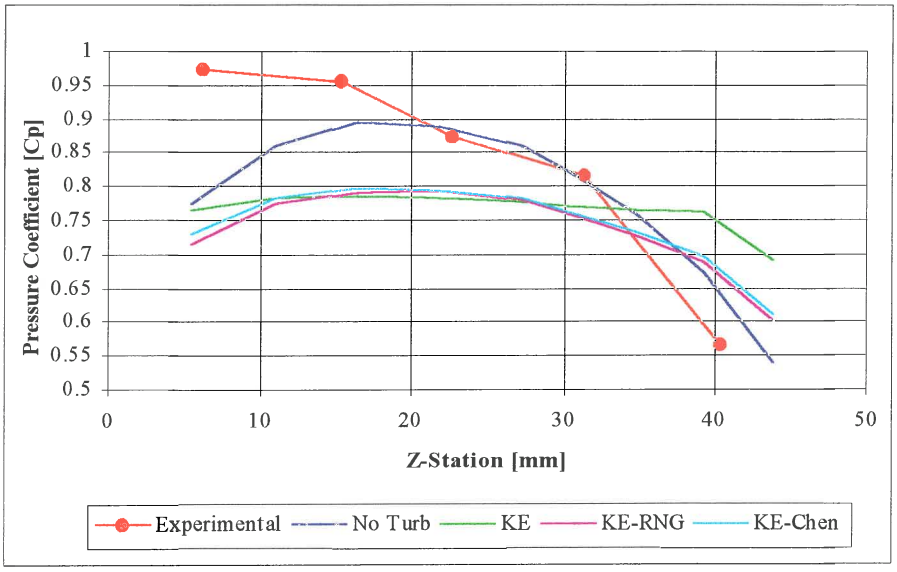

Figure 4-10 - BMW Nose: CFD Turbulence model comparisons

The stagnation point indicated by pressure coefficients close to unity is characterised by areas of low Reynolds-Number flows. This possibly accounts for the poor performance of the High Reynolds-Number turbulence models in this area. The additional terms in the dissipation and related closure terms of the RNG and Chen models as discussed in section 2.3.3.1 seems to improve the performance of these models compared to the standard k-ε model.

On the upper surface of the model, as shown in Figure 4-11, the four numerical models are in good agreement with each other until the leading edge of the roof. The overriding positive pressure gradient is the most likely cause for the agreement. Absolute correlation to the experimental case is however, less positive. The pressure coefficients are under-estimated by more than 0.5 in some cases. Despite this, the correct pressure trends, such as the accelerated flow over the leading edge of the bonnet, the slope change at the bottom of the windscreen and the acceleration over the windscreen, are still predicted by all the models.

From the roof leading-edge rearwards, overall correlation is less favourable. Although the laminar model follows the experimental data the closest, the pressure drop induced by the

negative gradient at the rear window is underestimated by this model. The turbulence models, as expected, capture the change in gradient with higher accuracy.

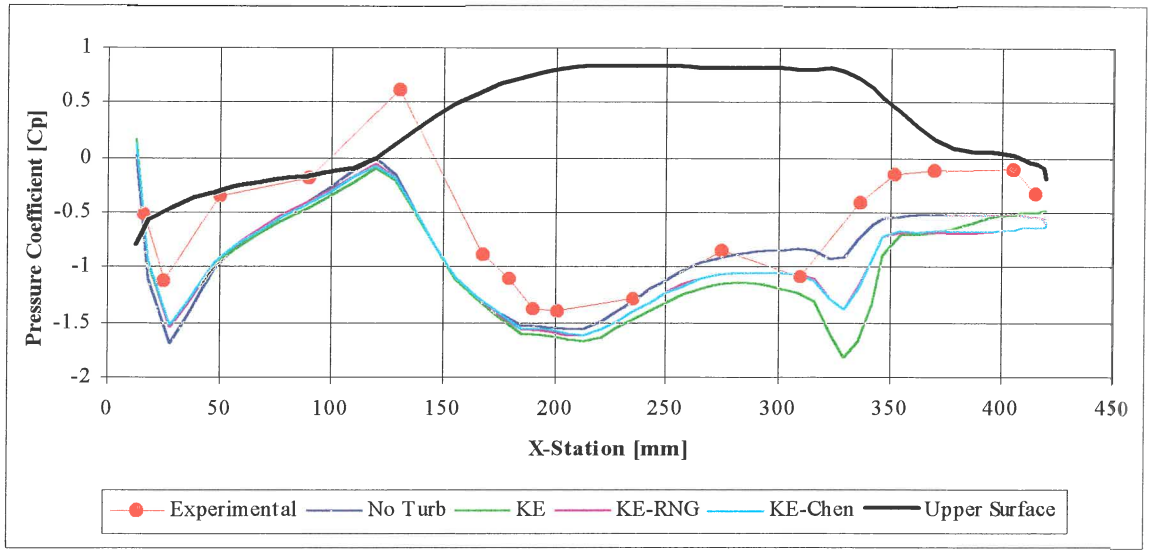

Figure 4-11 BMW Upper surface: CFD Turbulence model comparisons

The standard k-ε model overestimates the pressure recovery on the boot. Here, the RNG and Chen models perform better. These two models seem to be in very close agreement over the entire upper surface of the car.

Generally speaking it can be seen that the turbulence-model pressures are underestimated over the entire upper surface. One explanation for this can be the conservative calculation of the energetic turbulent boundary layer. This can possibly be rectified by increasing the turbulence intensity of the models. The incorrect location of the stagnation point on the nose can also be cited as one of the reasons for these inaccuracies.

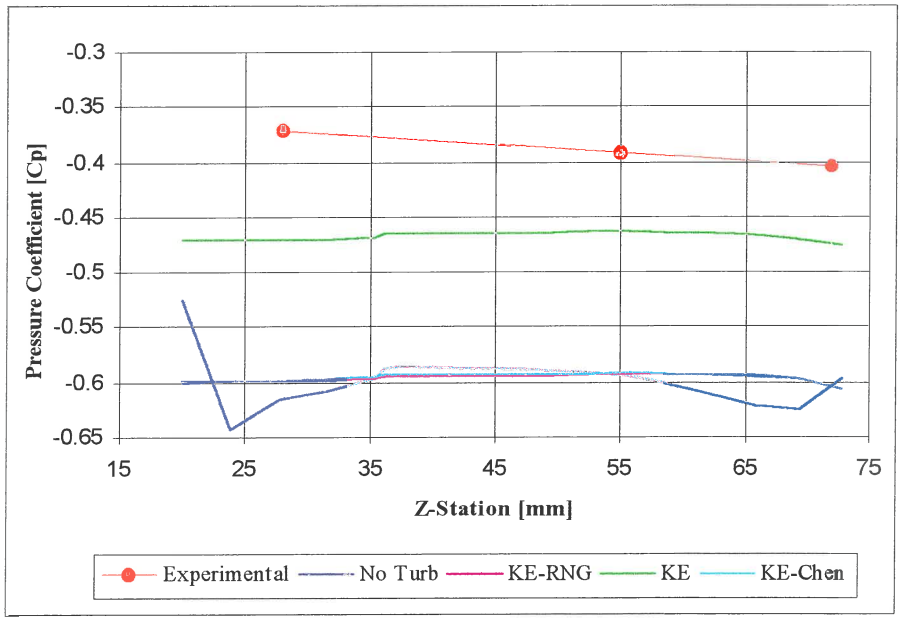

Figure 4-12 BMW Rear: CFD Turbulence model comparisons

At the rear of the vehicle, the flow is highly turbulent, completely separated and is characterised by large regions of re-circulating flow[8,16,18]. It is therefore not surprising that the turbulence models and in particular the standard k-ε model, out-perform the laminar model significantly. Although the RNG and Chen models produce results of similar magnitude to the laminar case, their pressure profiles agree better with the experimental data. As expected, the laminar model is poorly suited for the flow region presented in Figure 4-12.

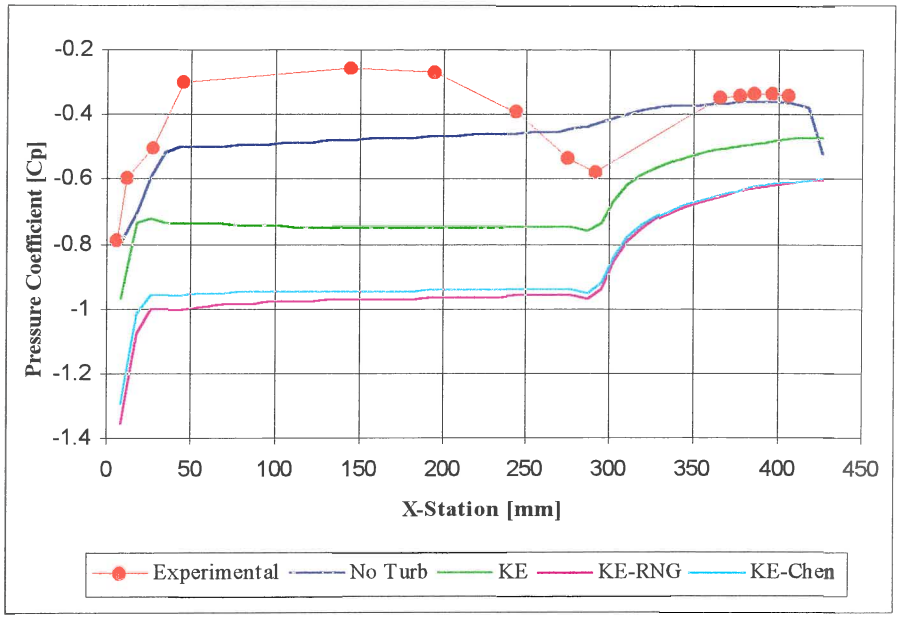

Figure 4-13 BMW Floor: CFD Turbulence model comparisons

As stated at the beginning of this chapter, this investigation was founded on the poor levels of numerical correlation in the F1 study of section 3.3. In Chapter 3 it was concluded that the absence of components such as the front splitter and rear wing had a major role to play in achieving correlation. This investigation was aimed at addressing this problem by simulating the centre-line profile of a complete vehicle.

Comparing Figure 3-24 of section 3.3 to Figure 4-13, one can see that by simulating the complete centre-line contour of the BMW, correlation has been increased in the front-splitter area. The effect of the front splitter, is clearly visible in Figure 4-13. The standard k-ε model renders the best solution in this region.

The greatest concern however, is the apparent inability of the CFD models to take the effect of the rear diffuser and its interaction with the rear end of the car into consideration. The inaccurate linear shape of the mid-section profile and the incorrect prediction of the diffuser-induced pressure drop were first observed in Figure 3-24. It seems that despite inclusion of the complete centre-line profile, the accuracy of the floor simulation has not really increased.

The findings of the experimental F1 study show that external parameters such as variations in ride height, front-flap angle adjustments and even the effect of the wheels, do not induce changes in the surface pressures which are similar in magnitude to the numerical discrepancies. This is also seen in Figure 4-8 where the removal of a relatively large GF from the rear end of

the BMW, does not produce pressure differences similar to those predicted by the CFD models. It therefore seems unlikely that the absence of the 3D flow field is the cause of the poor numerical results under the vehicle. The roots of the fundamental correlation discrepancies therefore seem to point towards problems with the numerical simulation techniques.

Two main areas can be highlighted where potential gains can be realised. These are:
- The numerical grid or computational domain
- The turbulence models and related parameters

As the extent and time scales involved in realising these potential improvements were unknown, it was decided to conclude this study by setting out guidelines for a new study. This discussion includes the results of three further simulations. The first investigated the effect of grid density while the other two were directed towards the effect of turbulence parameters.

4.2.3 Future Work

The contents of this section is aimed at outlining an approach which could be followed to improve the correlation between the numerical simulation of the centre-line profile of the $1/12^{th}$ scale BMW model and the related experimental results. The topics covered in this section are:
- The computational domain
- Turbulence models and related parameters

In conclusion, the influence of the 3D experimental flow field on the 2D simulation is also discussed as it is appreciated that these factors will become significant once the accuracy of the CFD model is increased.

4.2.3.1 The Computational Domain

As a first step to addressing the problem of the inaccurate computational domain, the effect of increasing the number of grid cells has to be investigated. A grid-independent solution was not obtained at the outset of the investigation, as it was felt that the grid resolution was high enough to obtain an estimate of the computational accuracy.

As an indication of the effect that grid density can have on the solution, the number of grid cells under the car was doubled. The entire grid was not modified to minimise grid generation and computational costs. The floor area was selected as it was here (Figure 4-13) where the poorest correlation existed. The results as shown in Figure 4-14 are compared to the solution of the unmodified grid and to the experimental data.

From Figure 4-14 it can be seen that the higher cell density under the floor has changed the solution slightly. Improvements were however, achieved with mixed success. Accuracy in the front-splitter area decreased. A marginal improvement is seen in the centre-floor section and at the entrance to the diffuser.

Further increases to the grid density or grid spacing in this area might improve the solution but it is suggested that this is performed in conjunction with refinements around the entire vehicle. Once a grid-independent solution has been reached, the far-field grid should then be investigated. The cycle of far-field near-field optimisation should be repeated at least once to ensure a truly grid-independent solution.

It is further suggested that the grid-optimisation process is performed using one of the standard STAR turbulence models, as the laminar grid, although important in determining the effect of turbulence, has been shown to be unsuitable for the flow around the BMW.

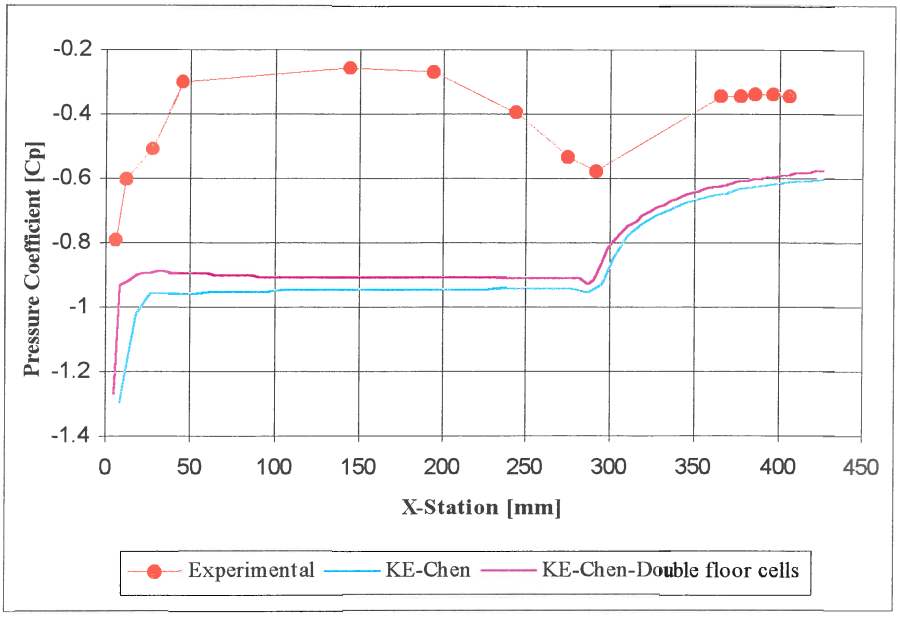

Figure 4-14 Effect of doubling the grid cells beneath the floor

If the optimised grid results in excessively skew cells, then the use of the SIMPISO algorithm, which is more robust than the SIMPLE method for severely distorted meshes, should be considered.

Once grid independence has been demonstrated, the investigation into the effects of turbulence models and related parameters has to be continued.

4.2.3.2 Turbulence Models and Related Parameters

The selection of the correct turbulence model is a difficult decision to make. It can be seen from Figure 4-10 to Figure 4-13 that the three STAR-CD models out-perform each other in different areas. Correlation in the nose area as shown in Figure 4-10 suggests that the standard k-ε model is the least suitable. Other areas such as the upper surface (Figure 4-11) and the rear end (Figure 4-12) indicate that this model is more suitable.

The choice of the correct turbulence model is complicated even further when the user definable mixing length and turbulence intensity are introduced as variables. To demonstrate this, the turbulence parameters of the standard k-ε model were varied and simulated as described in Table 4-5.

Turbulence Intensity	Mixing Length	
	0.01	0.005
0.1	Computed	-
0.01	Computed	Computed

Table 4-5 Variation of Standard k-ε parameters

The results of the simulations as outlined in Table 4-5 are compared to the experimental case in Figure 4-15.

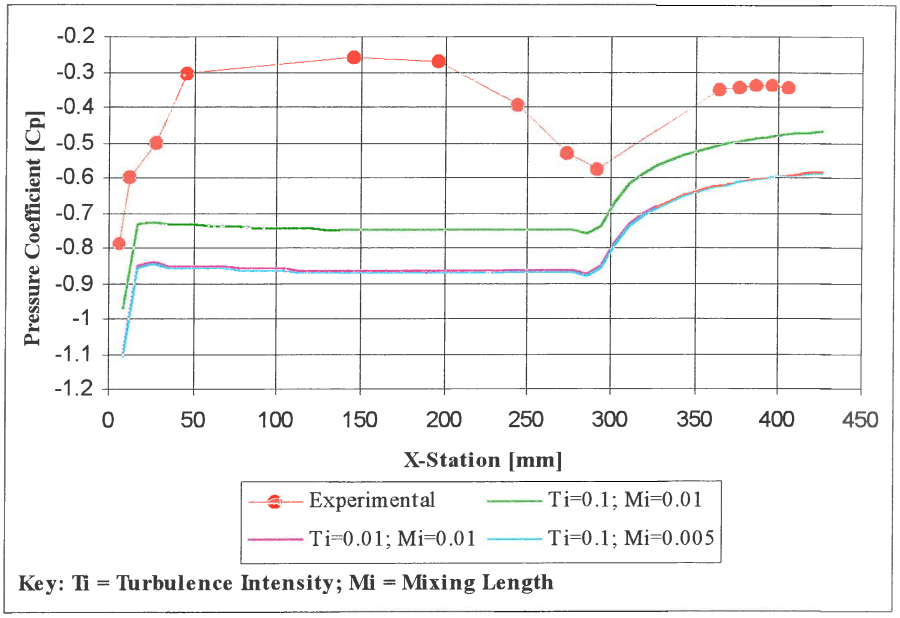

Figure 4-15 BMW Floor: Variation of k-e turbulence parameters

From Figure 4-15 it can be seen that the turbulence intensity has a more significant effect than the mixing-length parameter. It is also evident that the pressure profile of the mid-floor section remains almost unchanged. The results suggest that the intensity should be increased in the floor area. However, examination of the results above the vehicle, as presented in Figure 4-16, seem to indicate the opposite.

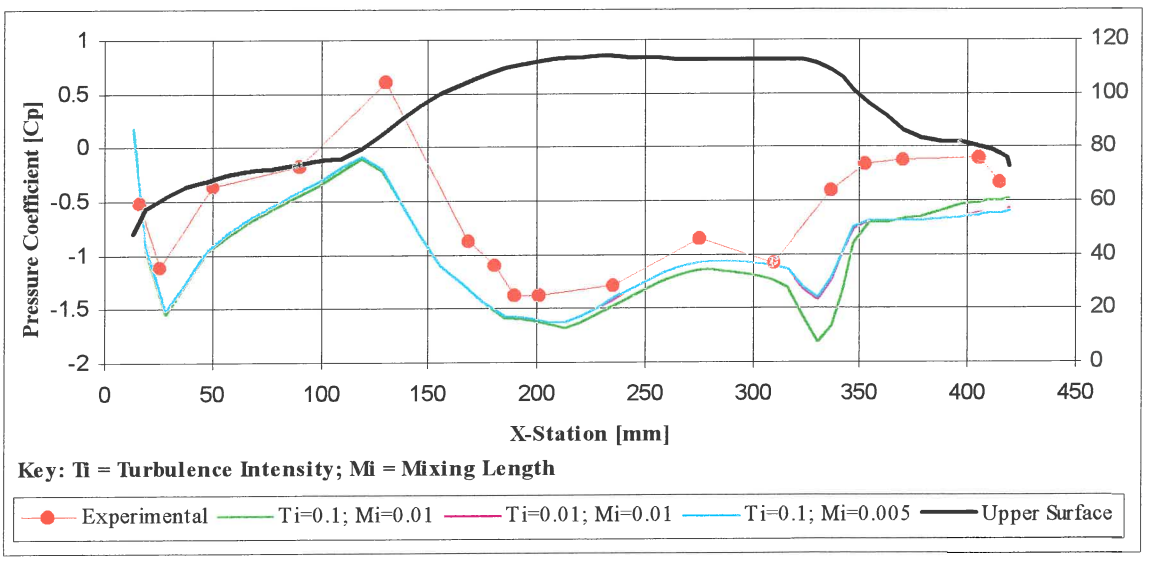

Figure 4-16 BMW Upper Surface: Variation of k-e turbulence parameters

The sensitivity of the simulations to changes in the turbulence parameters are highlighted when the coefficients of lift and drag are calculated by surface integration. As shown in Table 4-6 the lift coefficient can be changed by almost 60% by reducing the turbulence intensity by a factor of 10. The drag coefficient is less sensitive to these changes. This is to be expected as

the length to height ratio of the car suggests a greater sensitivity to pressure changes affecting forces in the direction normal to the free stream flow.

Turbulence Parameters for the k-ε model	Change in Drag Coefficient [% Δ CD]	Change in Lift Coefficient [% Δ CL]
Turbulence Intensity = 0.1 Mixing Length = 0.01	0	0
Turbulence Intensity = 0.01 Mixing Length = 0.01	7.17	-59.14
Turbulence Intensity = 0.1 Mixing Length = 0.005	7.29	-59.14

Table 4-6 Sensitivity of the solution to changes in turbulence parameters

The choice of the most representative turbulence model should only be made after an independent investigation of all three STAR models. The discussion in section 4.2.2.1 indicate that the results obtained from the standard k-ε model are unique when compared to the RNG and Chen models. This conclusion is however, only likely to hold while identical turbulence parameters are used. Comparing the k-ε model with a turbulence intensity of 0.1 to the RNG model with an intensity of 0.01, one can see from Figure 4-17, that the two models, despite their mathematical differences as described in section 2.3.3, are now in close agreement.

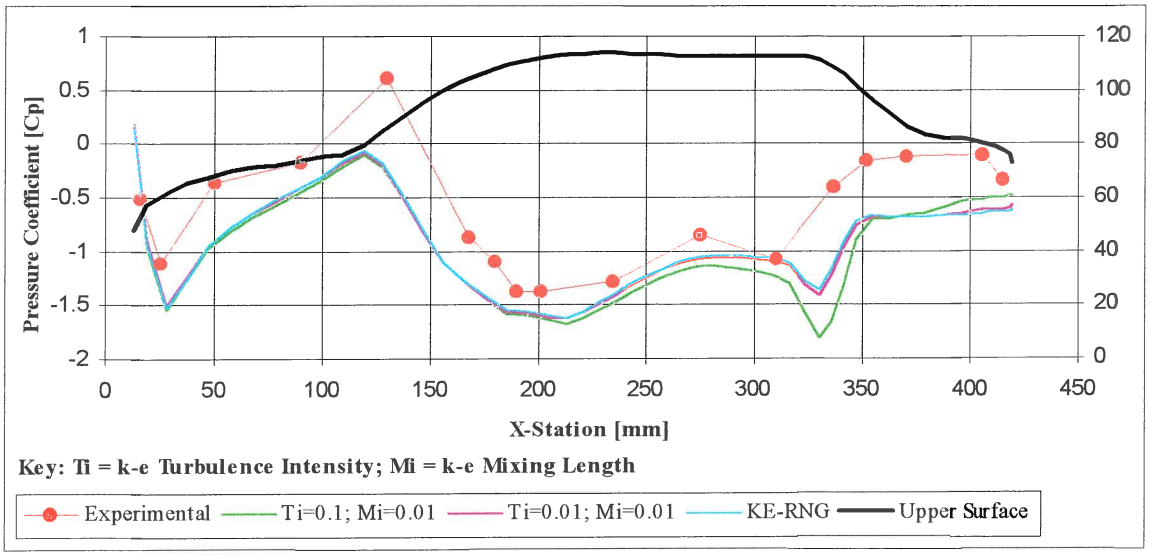

Figure 4-17 The effect of turbulence intensity on different turbulence models

As discussed in section 2.3.3 Cambers and Wilcox[34] found that the k-ε model and its derivatives were not suitable for flows where adverse pressure gradients existed. If these findings are seen to hold for the flow around the BMW, then an alternative approach such as the SST model of Menter[4] as discussed in section 2.3.3 and described in Appendix A might be more suitable. This model was specifically designed to address the deficiencies of the k-ε turbulence models.

4.2.3.3 The Effect of Excluding 3D Influences on the 2D Centre-Line Simulations

The 2D nature of the numerical simulations presented in this study, did not account for the influence of the 3D flow-field, implicitly included in the experimental results. These effects

were not clearly defined in this study and should therefore be addressed in future investigations.

Deviations from the 2D centre-line flow-case, assuming a symmetrical geometry along the centre-line of the vehicle, can be attributed to the influence of the wheels as well as the pressure differential that exists between the sides and the upper and lower surfaces of the vehicle.

In section 3.1.2.5 the effect of the wheels on the underbody flow-field was demonstrated for an open-wheel racing car. Although wheel-well flow patterns are very complicated and highly three dimensional for closed wheel cars, the effects of the wheels can be eliminated by removing the wheels and sealing the wheel-wells.

The interaction between the vehicle sides and the upper and lower surfaces are less easily neutralised. From Figure 3.7 and Figure 3.8 it can be seen that the higher side wall pressure causes an influx of air beneath the car. The net effect of this pressure increase under the floor on the centre-line is not clear. The vortices induced by the rear diffuser for both experimental models reduces the pressure in the diffuser area and therefore also influences the base pressure. These effects can be reduced by increasing the width of the vehicle until the centre-line pressure becomes insensitive to the side-wall pressures. An alternative approach would be to induce a pseudo 2D flow field along the centre-line by installing vertical walls at an appropriate distance from the centre-line. These walls would have to extend in front and behind the vehicle so that pressure differentials between the inboard and outboard side would not induce the formation of vortices in the test area. The y-position of these boards should also take the effect of boundary layer formation along their sides into account.

4.3 Conclusion

The aim of this investigation was to determine the accuracy with which a centre-line numerical simulation could be used to predict the pressure distribution on the centre line of a racing car. This was an extension of the computational work performed on the floor of the Parmalat Forti Ford F1 racing car in Chapter 3.

A $1/12^{th}$ scale model of a Generic BMW Touring car was selected for this investigation as it provided an ideal balance between the experimental and numerical detail, the costs and the efficiency with which results could be obtained.

The accuracy of the simulated results was verified using experimentally measured data. The data was obtained by building a model of the BMW, fitting it with surface-static pressure ports and testing it in a stationary-road closed-return wind tunnel. The measurements required for the computational investigation were made after repeatability and Reynolds-Number independence had been established. The experimental investigation was also used to establish a link with the F1 investigation by comparing the floor-pressure distributions of each case. It was found that the pressure plot under the BMW was in good agreement with the Forti distribution. As expected, the characteristic shape of the distribution under the open-wheel racing car was more pronounced and at a significantly lower average pressure.

The experimental investigation was also used to demonstrate and explain the phenomena responsible for rear downforce on sedan-based racing cars.

The numerical investigation was based on the centre-line profile of the wind-tunnel model. The grid was constructed using PRO-STAR. The effect of the three high Reynolds-Number turbulence models included in the STAR-CD software was investigated. These were compared to a laminar flow case and to the wind-tunnel results. It was found that although correlation exists in certain areas, the poorest correlation is found beneath the floor. This is ascribed to inaccuracies in the numerical procedures.

The combination of the inaccurate computational techniques and the varying success of the different turbulence models meant that satisfactory correlation could not be obtained. To address these deficiencies, an outline was laid down for a new study, aimed at improving the numerical model. It was suggested that by improving the mesh density and by altering the turbulence parameters, correlation could be improved. These suggestions were substantiated by further simulations. The use of turbulence models more suited to adverse pressure gradients was also included in the recommendations.

It was also shown that by varying the turbulence parameters, two different variations of the k-ε model could be tuned to predict similar results.

A short discussion on the influence of the 3D flow-field on the centre-line simulations conclude this chapter.

5. CONCLUSION

Race car aerodynamics has been transformed over the last four decades from a "cottage" industry, by designers like Colin Chapman who had the ingenious idea of reclining the drivers seat to reduce the frontal area, to a highly technical and sophisticated industry. Radical improvements of the past such as the introduction of wings or ground effects are rarely seen in the modern racing industry. Vast amounts of resources are now spent on obtaining the smallest advantage over the closest competitor. This is partly due to the law of diminishing returns but also due to the continuously shrinking size of the aerodynamic rule box. This was the case in 1995 when large chunks were taken out of the F1 rule box by the F.I.A. One of the areas that was significantly affected was the floor of the racing car. The flat-bottomed cars of the 1994 season were transformed to stepped-bottomed vehicles by removing two rectangular blocks, one on either side of the centre line, from the rule box. Such changes challenge the aerodynamicist to limit and neutralise the negative effect of the rule changes on lap times. As a first step to curbing the aerodynamic damage in a particular area, in this case the floor, the impact of the rules on the flow had to be established. An investigation into the flow beneath the floor of an F1 car was therefore launched.

The aim of this study was to investigate the flow patterns beneath a 30% scale model of the Parmalat Forti Ford FG01-95 Formula One racing car by using experimental and numerical methods. The experimental aim of the investigation was to determine the elements of the car, external to the floor, which were dominant in producing the flow-field patterns beneath the car. The experimental data was also used to investigate the numerical accuracy of simulating the centre-line profile of the floor.

The experimental results were obtained by building the 30% scale model, fitting the floor with static-surface pressure ports and testing it in the rolling-road LWST of the CSIR, South Africa. The results showed that the centre-line pressure profile characteristic to flat-bottomed racing cars was still clearly visible. It was found that the wheels were dominant in modifying the pressure distribution under the floor. It was further shown that only the front or rear wheel sets were required to induce these changes.

The numerical investigation was aimed at reproducing the wind-tunnel results by imposing experimentally measured boundary conditions on the grid of the centre-line profile of the isolated racing-car floor. The grid was constructed by using an algebraic grid generator and the simulations were performed using two CFD codes. One was an in-house code using Roe's flux difference splitting method and the other employed the SIMPLE algorithm of STAR-CD. It was found that although the correct trends could be observed when the ride heights were modified, absolute correlation could not be achieved. The absence of components such as the front splitter and rear-wing assembly were sited as the most likely cause for the discrepancies.

To increase the amount of model detail in the computational simulations, a new investigation was launched. In this investigation the complete centre-line profile of a $1/12^{th}$ scale generic model of a BMW Touring Car was used. The data for the numerical correlation was obtained from experimentally measured static-surface pressures. The stationary-floor wind tunnel at the University of Pretoria in South Africa, was used to measure the pressures on the centre-line around the circumference of the scale model. The experimental results were also used to establish a link with the F1 investigation by comparing the centre-line floor pressure

distribution of the two cases. By adding a Gurney Flap to the rear of the BMW the principles at play when generating rear downforce for sedan-based racing cars were also demonstrated.

The numerical BMW grid was constructed using PRO-STAR and solutions were obtained using the SIMPLE algorithm of STAR-CD. The results of three different k-ε turbulence-model simulations showed that despite limited success in certain areas around the vehicle, the inclusion of entire vehicle profile did not significantly increase correlation. The poor correlation was attributed to inaccuracies in the numerical methodology. It was proposed that another investigation, aimed at improving the numerical simulations, was required but that this study went beyond the scope of this script. Guidelines for the new investigation, based on the results of three additional simulations, were laid down. The related discussions suggested that a refined grid and a study into the effect of the user-definable turbulence parameters might improve the solution. It was also proposed that if the three turbulence models were found to be unsuitable, a more appropriate model such as the SST model of Menter should be used.

It is the author's belief that, although accurate numerical correlation could not be established in this study, CFD would, like wind tunnels, soon become an essential tool in the race-car aerodynamicist's quest for glory.